Cell

Article

Genome sequences of extant and extinct gibbons reveal their phylogeny, demographic history, and conservation status

Graphical abstract

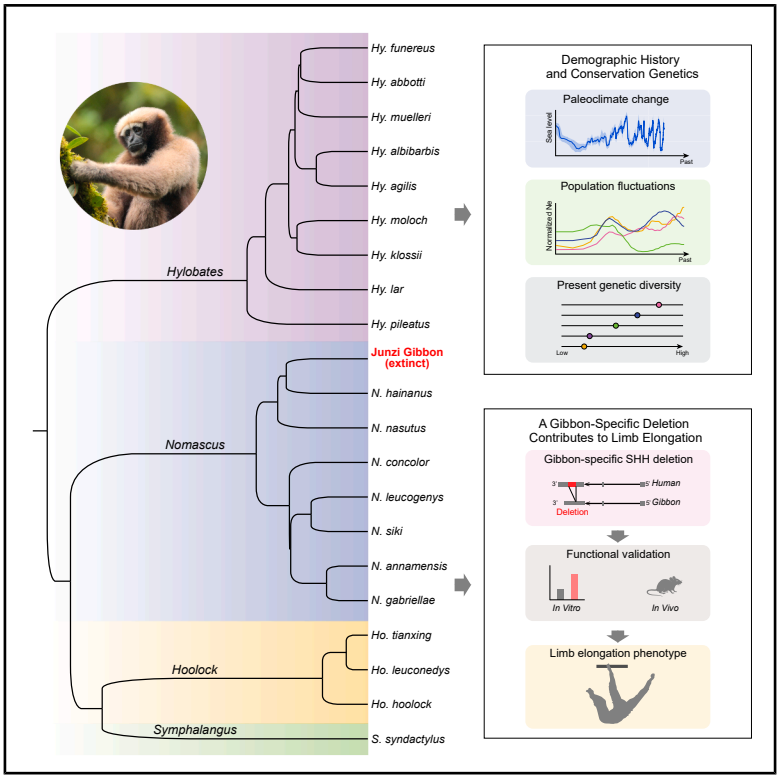

Highlights

- Robust genomic analyses resolve contentious gibbon phylogeny at genus and species levels
- Ancient mitochondrial DNA reveals the extinct *Junzi imperialis* is a species of *Nomascus*
- Genomic history reveals climate impacts and informs conservation of threatened gibbons
- A gibbon-specific deletion in an *SHH* regulatory element contributes to limb elongation

Authors

Sheng Wang, Zehui Chen, Ayun Luo, ..., Pengfei Fan, Qiaomei Fu, Dong-Dong Wu

Correspondence

fanpf@mail.sysu.edu.cn (P.F.), fuqiaomei@ivpp.ac.cn (Q.F.), wudongdong@mail.kiz.ac.cn (D.-D.W.)

In brief

This study presents a comprehensive evolutionary history of gibbons by resolving their contentious phylogeny, reclassifying an extinct species with ancient DNA, and identifying a structural variant potentially contributing to their limb elongation.

Wang et al., 2026, Cell *189*, 34–51
January 8, 2026
https://doi.org/10.1016/j.cell.2025.10.016

CellPress

CellPress

Cell

Article

Genome sequences of extant and extinct gibbons reveal their phylogeny, demographic history, and conservation status

Sheng Wang,[1,17] Zehui Chen,[2,17] Ayun Luo,[1,3,17] Xinran You,[1,17] Andrew C. Kitchener,[4,5,17] Xiaolong Tu,[1,3,17] Mukesh Thakur,[6] Govindhaswamy Umapathy,[7] Songmei Hu,[8,9] Tianen Zhang,[10] Yingqi Zhang,[2] Siqiong Liu,[2,3] Yan Ding,[10] Feng Liu,[2] Qingyan Dai,[2] Xiaotian Feng,[2] Lei Li,[11] Yue Pan,[2] Ming Zhang,[12] Christian Roos,[13,14] Pengfei Fan,[15,*] Qiaomei Fu,[2,3,*] and Dong-Dong Wu[1,16,18,*]

[1]State Key Laboratory of Genetic Evolution & Animal Models, Kunming Natural History Museum of Zoology, Kunming Institute of Zoology, Chinese Academy of Sciences, Kunming 650223, Yunnan, China

[2]Key Laboratory of Vertebrate Evolution and Human Origins, Institute of Vertebrate Paleontology and Paleoanthropology, Chinese Academy of Sciences, Beijing 100044, China

[3]University of Chinese Academy of Sciences, Beijing 100049, China

[4]Department of Natural Sciences, National Museums Scotland, Chambers Street, Edinburgh EH1 1JF, UK

[5]School of Geosciences, University of Edinburgh, Drummond Street, Edinburgh EH9 3PX, UK

[6]Zoological Survey of India, New Alipore, Kolkata 700053, West Bengal, India

[7]Laboratory for the Conservation of Endangered Species, CSIR-Centre for Cellular and Molecular Biology, Uppal Road, Hyderabad 500007, India

[8]Key Laboratory of Archaeological Sciences and Technology, Shandong University, Ministry of Education, Qingdao 266237, China

[9]Institute of Cultural Heritage, Shandong University, Qingdao 266237, China

[10]Shaanxi Academy of Archaeology, Xi'an 710054, China

[11]Chongqing China Three Gorges Museum, Chongqing 400015, China

[12]School of Cultural Heritage, Northwest University, Xi'an 710069, China

[13]Primate Genetics Laboratory, German Primate Center, Leibniz Institute for Primate Research, Göttingen, Germany

[14]Gene Bank of Primates, German Primate Center, Leibniz Institute for Primate Research, Göttingen, Germany

[15]School of Life Sciences, Sun Yat-sen University, Guangzhou 510275, China

[16]National Resource Center for Non-Human Primates, Kunming Primate Research Center, and National Research Facility for Phenotypic & Genetic Analysis of Model Animals (Primate Facility), Kunming Institute of Zoology, Chinese Academy of Sciences, Kunming 650107, Yunnan, China

[17]These authors contributed equally

[18]Lead contact

*Correspondence: fanpf@mail.sysu.edu.cn (P.F.), fuqiaomei@ivpp.ac.cn (Q.F.), wudongdong@mail.kiz.ac.cn (D.-D.W.)

https://doi.org/10.1016/j.cell.2025.10.016

SUMMARY

Gibbons (family *Hylobatidae*), small apes closely related to humans and great apes, remain understudied despite their threatened status. Here, we present extensive genomic resources, including chromosome-level reference genomes, whole-genome resequencing of 18 extant species, and mitochondrial genomes from 3 ancient samples. Using whole-genome alignments, we resolve the debated phylogeny of the four genera as (*Hylobates*, (*Nomascus*, (*Symphalangus*, *Hoolock*))). Phylogenetic analyses based on the ancient mitogenomes place the extinct *Junzi imperialis* within *Nomascus*, refuting its status as a distinct genus. Conservation genomics and ecological niche modeling analyses suggest historical dynamics in gibbon population size and habitat suitability, which are consistent with the potential impacts of past climate change. Through comparative genomics and transgenic mouse experiments, we identify a 205-bp deletion in the Sonic Hedgehog (SHH) gene associated with gibbons' elongated limbs. These findings advance understanding of gibbon evolution, biology, and conservation.

INTRODUCTION

Gibbons (family *Hylobatidae*) are a group of threatened primates endemic to the tropical forests of Southeast Asia.[1,2] Gibbons exhibit various characteristics distinct from other primates, including a unique combination of body size, morphology, anatomy, and behavior. In particular, gibbons display some specific adaptations for an arboreal lifestyle. For example, they have

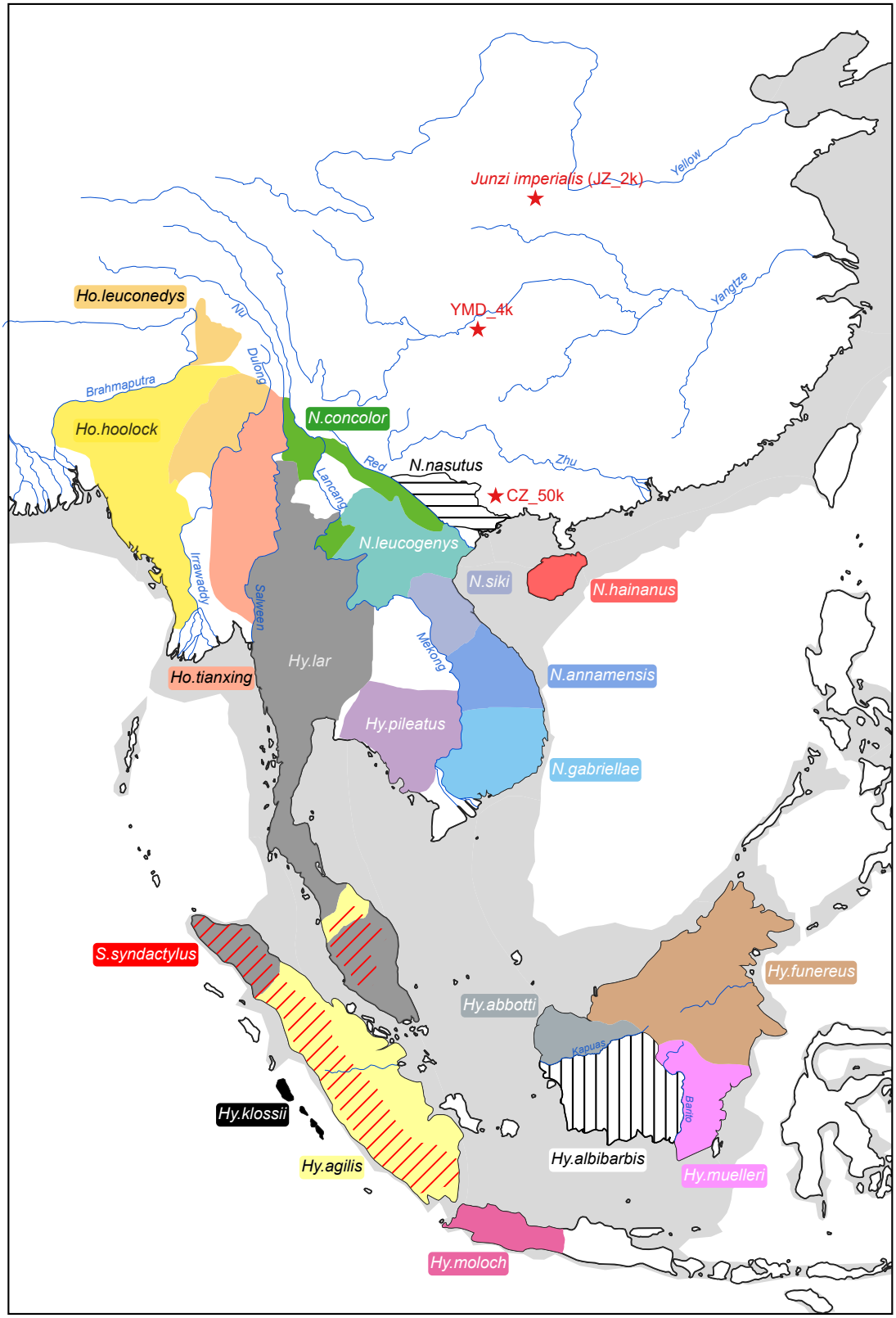

(legend on next page)

strong, long arms and hook-shaped hands for grasping branches, which enable them to perform a special locomotion called brachiation.[3] In addition, their shoulder joints are adapted to allow a greater range of motion when brachiating, and their legs are long and powerful for propelling and grasping. Despite many years of morphological and anatomical investigations, the genetic underpinning of their distinctive skeletons remains largely elusive.

Currently, 20 extant species in four genera (*Nomascus*, *Symphalangus*, *Hoolock*, and *Hylobates*) are recognized (Figure 1; Table 1).[1] However, additional genera and species occurred in ancient and historical times but are now extinct. For example, *Bunopithecus sericus* from Sichuan, China, probably dates back to the early-middle Pleistocene.[4] The extinct *Junzi imperialis* was identified based on the morphology of ancient remains found in the tomb of Lady Xia,[5–7] grandmother of China's first emperor, Qin Shihuang (259–210 BCE). Owing to their rarity and arboreal lifestyle, obtaining samples for genome sequencing is difficult, and hence, our knowledge and understanding of gibbons is still limited. One of the major controversies is the phylogenetic relationship among the four genera.[8–10] Despite numerous studies using morphological, behavioral,[11] genetic data,[12–15] and even genome resequencing data,[8–10] the branching pattern among the four genera remains unresolved, likely due to the rapid evolutionary radiation of gibbons and problems with incomplete lineage sorting (ILS).[8,16,17]

Despite tremendous conservation efforts, gibbons are still among the most threatened primates on earth, and some species are close to extinction. For example, two species, the white-handed gibbon, *Hylobates lar*, and the northern white-cheeked gibbon, *Nomascus leucogenys*, have been recently declared extinct in China because they have not been recorded in their southern Chinese habitat for more than a decade,[20,21] although they persist in parts of Southeast Asia. While human activities and environmental destruction are the primary drivers of gibbon endangerment,[22,23] conservation genomics gaining insight into their patterns of genetic diversity is crucial for assessing their vulnerability and could improve future conservation management strategies but remains largely unexplored.

In this study, we collected a comprehensive genomic dataset for gibbons, including genome sequencing data from 18 extant gibbon species (Tables 1 and S3), except two extant species (*N. nasutus* and *Hy. albibarbis*), primarily due to challenges in obtaining high-quality samples for whole-genome sequencing. We also successfully retrieved and analyzed ancient DNA from three Holocene and Pleistocene specimens, including the enigmatic *Junzi imperialis* and two other previously unidentified gibbons. Using this integrated dataset, we resolved the phylogeny of the 4 gibbon genera and reconstructed phylogenetic relationships among 18 extant gibbon species and three ancient samples. We then integrated conservation genomics analysis and ecological niche modeling to reveal the potential effects of climate change on the population dynamics of gibbons. Finally, through comparative genomics and functional validation in transgenic mice, we identified a 205 bp deletion in the Sonic Hedgehog (*SHH*) gene and demonstrated its potential role in causing the elongated limbs characteristic of gibbons. Overall, this study settles the long-standing phylogeny of gibbons, expands our knowledge of the mechanisms underlying their phenotypic evolution, and enhances our understanding of gibbon evolution and conservation.

RESULTS

Large-scale genome sequencing data for extant and extinct gibbons

In our previous primate genome project,[24,25] we released four *de novo* assembled genomes of gibbons, namely *Nomascus siki*, *Symphalangus syndactylus*, *Hylobates pileatus*, and *Hoolock leuconedys*, representing all four gibbon genera, using long-read sequencing technology (PacBio RS II or Nanopore PromethI ON). However, only *Hy. pileatus* harbors a chromosome-level assembly. Here, we generated Hi-C (high-throughput chromosome conformation capture) sequencing data[26] for *S. syndactylus* and *Ho. leuconedys* to anchor contigs to chromosomes (Figures S1A and S1B).[27] Additionally, by leveraging the synteny with *N. leucogenys* (Asia_NLE_v1), we refined the *N. siki* genome into pseudo-chromosomes.[28] Gene annotations were conducted through a combination of homology-based and *de novo* prediction approaches,[29,30] despite the absence of transcriptome data (Tables S1 and S2). These chromosomes enable us to investigate karyotype evolution of gibbons, which corroborates pervasive genome rearrangements and chromosome fusions/fissions among genera and species,[12] particularly in *Ho. leuconedys*. Notably, these chromosomal changes occur predominantly on autosomes rather than the X chromosome (Figure S1C). This relative stability of the X chromosome is likely attributable to factors such as its lower recombination rates compared with autosomes,[31] which reduces the opportunities for rearrangements, and potentially stronger purifying selection acting against structural changes on the X chromosome, contributing to its conserved synteny across mammals.[32]

In addition, we collected samples of 75 individuals representing 18 extant gibbon species, including 31 newly sequenced individuals. The genomes of these individuals were sequenced using a short-read sequencing platform (Illumina NovoSeq or Mouse Genome Informatics [MGI] DNBSEQ-T7) with an average depth of 28.0 (Tables 1 and S3). Furthermore, we successfully

Figure 1. Geographical distribution of extant and extinct gibbons

Red stars on the map mark the geographical locations of three ancient samples. YMD_4k: ~4,000-year-old gibbon sample from Yemao Cave, Qijiang District, Chongqing, China. CZ_50k: ~50,000-year-old gibbon sample from Longlinshan Cave, Manluxincun, Chongzuo, Guangxi Province, China. JZ_2k: *Junzi imperialis* from Shenheyuan tomb (from a ~2,200- to 2,300-year-old tomb possibly belonging to Lady Xia, grandmother of China's first emperor, Qin Shihuang (259–210 BCE), Changan District, Shaanxi Province. Species distributions were adapted from previous studies.[1,18,19] The additional land area at the historical minimum sea level during the Last Glacial Maximum (LGM, ~19–26 kya) is shown in light gray. Geographical information on land and rivers was obtained from Natural Earth (https://www.naturalearthdata.com/).

See also Figure S1.

Table 1. Species information of extant gibbons

Genus	# Chromosomes (2n)	Scientific name	Common name	Abbr.	IUCN categories[a]	# New sequencing sample/# total sample of nuclear genome (mean depth)	# New sequencing sample/# total sample of complete mitochondrial sequence
Hylobates	44	*Hy. pileatus*	pileated gibbon	HPI	EN	4/5 (37.4)	4/5
		Hy. lar	white-handed gibbon	HLA	EN	3/5 (34.9)	3/4
		Hy. moloch	moloch gibbon	HMO	EN	1/3 (33.2)	3/4
		Hy. klossii	Kloss's gibbon	HKL	EN	1/2 (31.3)	1/2
		Hy. agilis	agile gibbon	HAG	EN	1/3 (32.5)	2/3
		Hy. muelleri	Mueller's gray gibbon	HMU	EN	1/3 (31.3)	2/2
		Hy. funereus	east Bornean gray gibbon	HFU	EN	1/1 (25.9)	1/1
		Hy. abbotti	Abbott's gray gibbon	HAB	EN	1/2 (30.4)	2/2
		Hy. albibarbis	Bornean white-bearded gibbon	HAL	EN	–	0/1
Nomascus	52	*N. leucogenys*	northern white-cheeked gibbon	NLE	CR	2/13 (21.3)	11/12
		N. siki	southern white-cheeked gibbon	NSI	CR	2/3 (43.2)	2/3
		N. concolor	western black-crested gibbon	NCO	CR	1/2 (18.6)	2/3
		N. annamensis	northern yellow-cheeked gibbon	NAN	EN	4/5 (24.9)	5/5
		N. gabriellae	southern yellow-cheeked gibbon	NGA	EN	1/4 (20.7)	3/4
		N. hainanus	Hainan gibbon	NHA	CR	1/1 (9.3)	1/1
		N. nasutus	eastern black-crested gibbon	NNA	CR	–	1/1
Hoolock	38	*Ho. hoolock*	western hoolock gibbon	HHO	EN	2/13 (27.2)	2/3
		Ho. leuconedys	eastern hoolock gibbon	HLE	VU	1/4 (25.9)	4/5
		Ho. tianxing	skywalker hoolock gibbon	HTX	EN	2/2 (32.6)	2/3
Symphalangus	50	*S. syndactylus*	siamang	SSY	EN	2/4 (33.4)	4/5

[a]VU, vulnerable; EN, endangered; CR, critically endangered.

retrieved ancient mitochondrial genomes from three key specimens (Figures 1 and S5A; Table S6). One sample (denoted as JZ_2k, ~2.2 thousand years ago [kya]) is from the described extinct species *Junzi imperialis*, which was proposed as a new genus based on morphology.[5] The other two represent previously unidentified gibbon specimens whose taxonomic affinities were unknown prior to this study: a ~4,000-year-old specimen from Yemao Cave, Chongqing (denoted as YMD_4k), and a ~50,000-year-old specimen from Longlinshan Cave in Chongzuo, Guangxi (denoted as CZ_50k). For these ancient samples, mitochondrial genomes were captured using an enrichment strategy at 5.3–63.9× depth, with average read lengths of 37.9–51.8 bp. The cytosine deamination (C to T) frequencies for fragments at the first position of the 5′ end from CZ_50k, YMD_4k, and JZ_2k samples were 6.0%, 6.6%, and 23.2%, respectively. By contrast, the 3′ end showed average frequencies of 28.0%, 25.8%, and 22.2% (Figure S5B; Table S7).

Whole-genome alignment of reference genomes clarifies the controversial phylogeny of the four gibbon genera owing to pervasive ILS

The phylogenetic relationships among the four genera have been debated for decades.[8–10,14,18,33] Even with recently available genome resequencing data, studies have drawn different

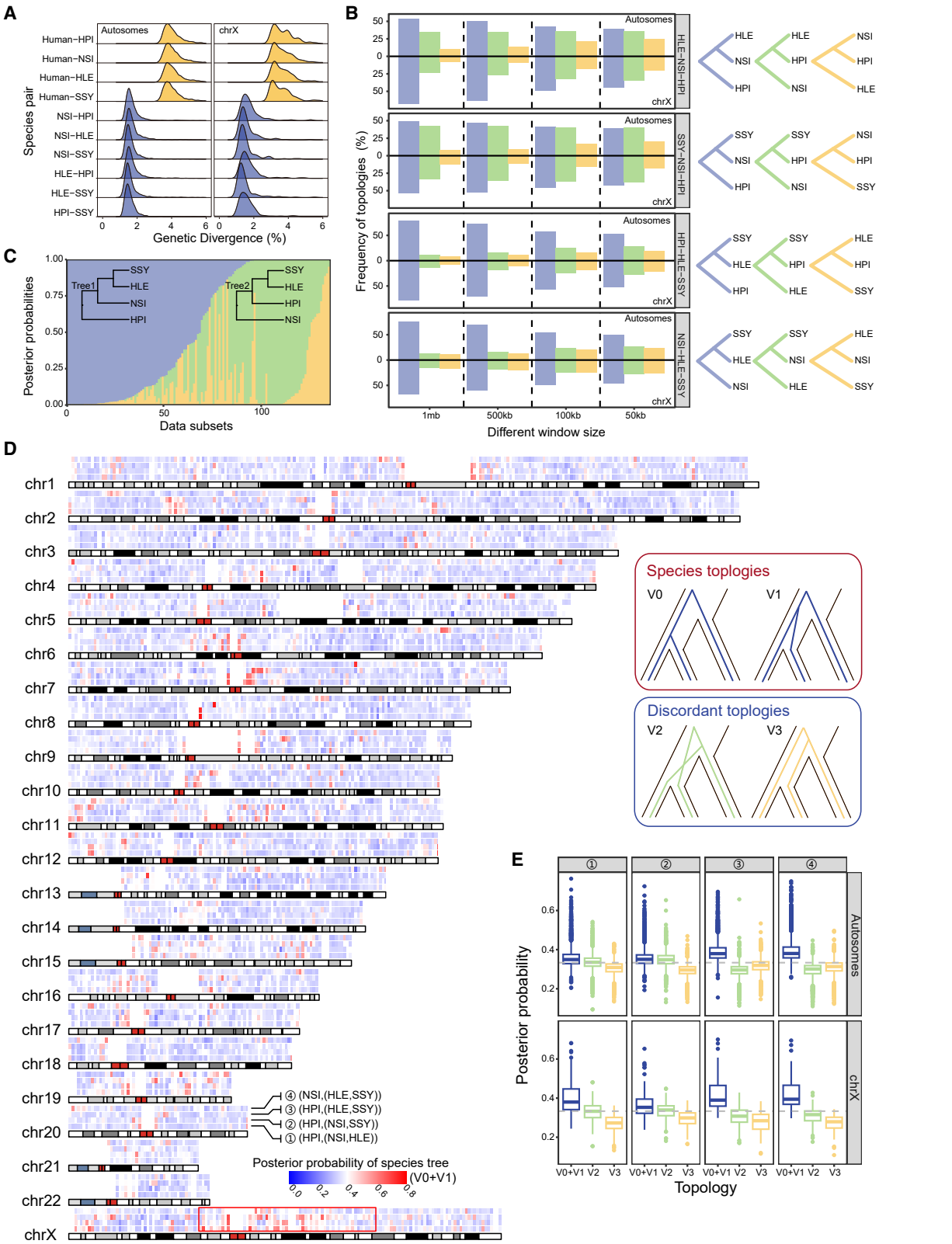

(legend on next page)

conclusions.[8–10] Given the absence of gene flow between different gibbon genera,[9] the observed phylogenetic discordance likely stems from ILS. ILS occurs when ancestral polymorphisms persist through speciation events and are randomly fixed in descendant lineages, leading to gene trees that differ in topology from the species tree. This phenomenon arises from coalescence events between lineages occurring deeper in time than the speciation event separating them.[34] ILS is expected to be particularly pervasive when the time between speciation events is short relative to the ancestral effective population size (N_e), as the timescale for coalescence is proportional to N_e (on the order of $4N_e$ generations), which occurred commonly during the rapid speciation process or when the ancestral effective population size was large.[35] Short internal tree branch lengths (see below) and similar genetic distances between any pair of the four gibbon genera (Figure 2A) indeed support the rapid speciation process of gibbons, as reported previously.[8,10]

Considering that previous phylogenetic reconstructions, based on variants identified through mapping short-read genomic data to the *N. leucogenys* reference genome,[8–10] may have introduced ascertainment bias, potentially leading to the exclusion of important variants,[36–38] we generated a whole-genome alignment of the four *de novo* assembled genomes to retrieve homologous sequences for phylogenetic analyses. To determine the genus-level species tree, we first constructed large-scale phylogenetic trees using multiple approaches (Figure S2). While prior studies debated two primary topologies: (*Hylobates*, (*Nomascus*, (*Hoolock*, *Symphalangus*))) (Tree1) and (*Nomascus*, (*Hylobates*, (*Hoolock*, *Symphalangus*))) (Tree2),[8–10,24] our analyses revealed more complex conflicting signals. The concatenation-based trees using 4-fold degenerate (4d) sites and coding sequences (CDSs) recovered both Tree2 and a third topology, ((*Nomascus*, *Hylobates*), (*Symphalangus*, *Hoolock*)) (Tree3), depending on whether autosomal or X chromosome data were used (Figures S3A and S3B; Table S4). This conflict was further evident in our sliding-window approach, where Tree3 emerged as the most frequent topology, with the other two balanced trees as the second and third topologies, particularly on autosomes (Figures S3C and S3D; Table S4).

The simple majority-vote method of using the most commonly observed gene tree as the species tree has a significant risk of yielding flawed outcomes, because the most probable gene tree may not match the species tree and is called an anomalous gene tree in the "anomaly zone,"[39–41] which occurs frequently in the situation of ILS. To resolve the species tree amidst this conflict, we therefore employed two independent methods that are theoretically robust to the anomaly zone and the high levels of ILS. First, we capitalized on the theoretical finding that phylogenies comprising three taxa are free of the anomaly zone.[39] We therefore performed an "anomaly-zone-free" analysis by systematically constructing trees for all four possible three-taxon combinations derived from the four gibbon genera. This approach yielded a remarkably consistent result: all four combinations exclusively recovered local topologies that were congruent with the overarching species tree topology of Tree1: (*Hylobates*, (*Nomascus*, (*Hoolock*, *Symphalangus*))) (Figure 2B; Table S4). Second, we inferred the species tree using a multispecies coalescent (MSC) model as implemented in the BPP program.[42] Unlike concatenation, MSC methods explicitly model the coalescent process underlying ILS, allowing for direct estimation of the species tree's posterior probability. This analysis provided strong statistical support for Tree1 as the most probable species tree, with a mean posterior probability of 0.48 for Tree1, which was higher than that of 0.37 for Tree2 (Figure 2C; Table S4). In conclusion, our systematical analyses indicate that the species tree of the four gibbon genera should be (*Hylobates*, (*Nomascus*, (*Hoolock*, *Symphalangus*))) (Tree1). This topology was therefore used in all subsequent analyses.

Having resolved the species tree, we next applied the coalescent hidden Markov model with ILS (CoalHMM-ILS)[43] to characterize the genomic landscape of ILS and to infer speciation times and ancestral population sizes. We analyzed the genome in the context of the four possible three-taxon combinations that can be derived from our four-taxon species tree (Figure 2D). This analysis revealed that most autosomal genomic regions display

Figure 2. Phylogeny among the four gibbon genera and ILS

(A) Ridgeline plots of pairwise genetic divergence between gibbon genera and between gibbons and humans. Divergence was calculated in non-overlapping 1 Mbp windows across the genome. Each row represents a specific species pair, with analyses performed separately for autosomes (left column) and the X chromosome (right column). The density distributions were plotted and estimated using a kernel density estimation (KDE) with a Gaussian kernel using the ggridges package in R.

(B) Bar plots of topology frequencies from anomaly-zone-free 3-taxa sliding-window phylogenetic analysis. The sliding-window phylogenies were performed on all four possible three-taxon combinations. The bar plots show the percentage of windows supporting each of the three possible topologies for each combination across four different window sizes (from 50 kb to 1 Mb) and different chromosome groups (all autosomes and the X chromosome).

(C) Stacked bar plot of posterior probabilities from BPP analysis. Each vertical bar represents one of 144 non-coding data subsets, with colors showing the posterior probability supporting either Tree1 ((Hy, (N, (S, Ho)))) in blue, Tree2 ((N, (Hy, (S, Ho)))) in green, or other topologies in orange.

(D) Genomic landscape of incomplete lineage sorting (ILS) under the resolved species tree (Tree1). The heatmap displays the local posterior probabilities of genomic windows supporting the species tree topology across all autosomes and the X chromosome estimated from ILS-CoalHMM. Each chromosome is represented by four heatmap rows, where each row corresponds to one of the four possible three-taxon species trees, as defined in the legend at the bottom right. Red indicates a high percentage of species tree topologies (low ILS), while blue indicates a low percentage (high ILS). The red solid box on the X chromosome highlights a large region of low recombination in the human genome (chrX: 46,912,276–110,795,819, GRCh38). The inset defines the four possible genealogies for a given species triplet, with V0 and V1 representing topologies concordant with the species tree, and V2 and V3 representing discordant topologies typically caused by ILS.

(E) Boxplots showing the distribution of posterior probabilities on concordant (V0 + V1) and discordant topologies (V2 and V3). For each 1 Mbp genomic window, ILS-CoalHMM estimated the posterior probability for each topology. The boxplots display the distribution of these probabilities from all windows, with each of the four main plots (labeled ①–④) corresponding to one of the specific three-taxon comparisons defined in (D).

See also Figure S3.

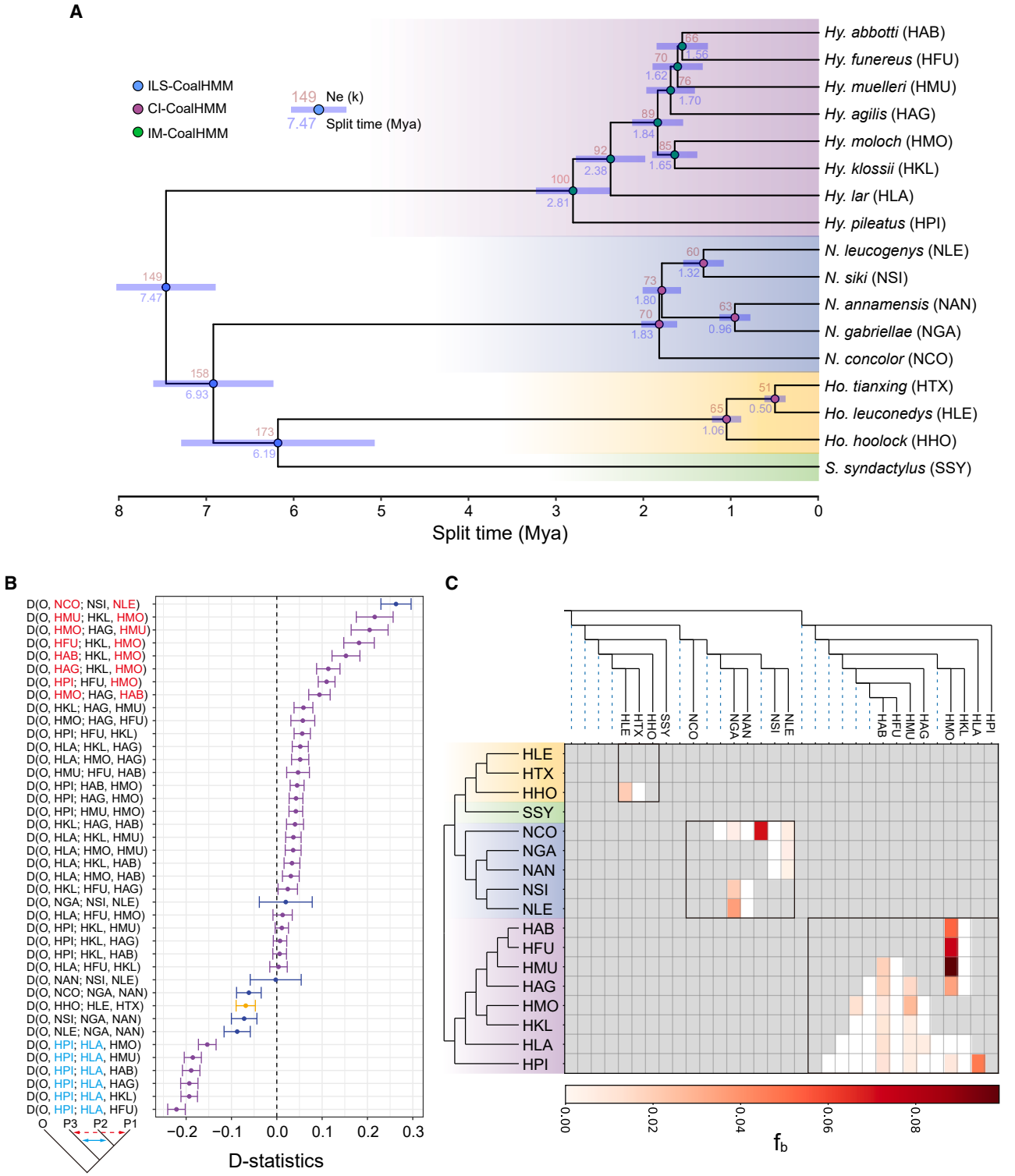

Figure 3. Gibbon phylogeny and gene flow among species

(A) Phylogeny and population demographic parameters of gibbon species harboring genome data. Divergence times (blue) and ancestral effective population sizes (red) are shown at the nodes. Horizontal bars represent the interquartile range of divergence times. The parameters were estimated using models tailored to different evolutionary scenarios. For inter-genus splits, ILS-CoalHMM was used to account for ILS. For intra-genus splits, parameters were estimated using the complete isolation CoalHMM (CI-CoalHMM) and isolation with migration CoalHMM (IM-CoalHMM) model to account for the potential effect of gene flow. The

(legend continued on next page)

high levels of ILS, as indicated by a high posterior probability of gene trees with discordant topologies relative to the species tree. By contrast, the X chromosome, particularly its low-recombination regions, exhibited significantly reduced levels of ILS (Figures 2D and 2E). Assuming a substitution rate of 1.0×10^{-8} per site per generation[8] and a generation time of 15 years,[44] our demographic modeling indicated a rapid radiation event among the four gibbon genera. The diversification of the four extant genera occurred over a condensed time frame of approximately 1.28 million years (from ~7.47 to ~6.19 mya) (Figure 3A). The ancestral effective population sizes (N_e) for the three ancestors were relatively large, with estimates of ~149,000 for the last common ancestor of all gibbons, ~158,000 for the *Nomascus-Hoolock-Symphalangus* common ancestor, and ~173,000 for the *Hoolock-Symphalangus* common ancestor (Figure 3A), closely matching those of humans and orangutans.[45,46] The large ancient population sizes and rapid speciation process are conducive to ILS as described above. Finally, using these ancestral population sizes and internal time spans according to the coalescent theory,[35] we estimate ILS probabilities of 59.0% and 57.0% between the three speciation events in the genera tree, which align with the mean genomic fragments of two discordant topologies (Figure 2E).

Phylogenomic analyses reveal species validity and gene flow within gibbon genera

In addition to resolving the branching pattern among the four gibbon genera, the phylogenetic relationships among gibbon species remain unclear due to the limited availability of whole-genome data for most species. After settling the phylogeny of the four genera, we reconstructed species-level phylogenetic relationships and estimated divergence times among gibbon species (Figure 3A) based on whole-genome resequencing data. This fundamental information is critical for understanding phylogeography, demographic history, and improving conservation strategies for these threatened species. We initially constructed neighbor-joining and maximum-likelihood phylogenetic trees to explore the genetic relationships among species within three genera (*Hylobates*, *Nomascus*, and *Hoolock*) using whole-genome variants (Figures 3A and S4). The branching pattern within *Hylobates* is consistent with previous results using mitochondrial and partial nuclear DNA.[44] *Hy. pileatus* (HPI) represents the most basal species, followed by *Hy. lar* (HLA). The remaining species form two distinct clades, one encompassing *Hy. moloch* (HMO) and *Hy. klossii* (HKL), and the other containing *Hy. agilis* (HAG), *Hy. muelleri* (HMU), *Hy. funereus* (HFU), and *Hy. abbotti* (HAB). Recently recognized as separate species, *Hy. abbotti* and *Hy. funereus*, together with *Hy. muelleri*, comprise the most closely related species. Within the *Nomascus* genus, we lack the nuclear genome of the eastern black-crested gibbon (*N. nasutus* [NNA]) and have only low-coverage genome of the Hainan gibbon (*N. hainanus* [NHA]). Therefore, we further sequenced the mitochondrial genome for *N. nasutus* (NNA) and assembled the mitochondrial genome from low-coverage genomic data for *N. hainanus* (NHA) for constructing phylogeny (Figure 4B). Mitogenome phylogeny shows that these two species (NNA and NHA) are the most basal among *Nomascus* species (Figure 4B). Overall, the phylogeny of species within genera is consistent with previously published results.[18]

Divergence times estimated from whole-genomic data support previous reports about multiple radiations in the evolutionary history of gibbons using mitochondrial DNA[18] (Figure 3A). The first radiation, involving the radiation of the four gibbon genera, occurred between ~7.47 and ~6.19 mya, while the second, spanning ~2.81 to ~1.56 mya, gave rise to extant *Hylobates* species and separated black-crested and light-cheeked gibbons (white- and yellow-cheeked gibbons) in *Nomascus*. Finally, *Hoolock* and light-cheeked gibbons diverged into separate species within the last 1 million years. In addition to these deeper divergences, the divergence times estimated between recently described species provide support for their taxonomic validity. The divergence times are consistent with their classification as distinct evolutionary lineages, thus providing crucial support for their species-level status (Figure 3A). For instance, the skywalker hoolock gibbon (*Ho. tianxing* [HTX]), the most recently described gibbon species, is distinguished from other hoolock species by a combination of coat color patterns, tooth morphology, and mitochondrial DNA sequences.[48] Our whole-genome analyses estimate the divergence time between *Ho. tianxing* and its closest relative, *Ho. leuconedys*, to be ~0.50 mya. A similar pattern is observed in other recently described species, such as *N. annamensis*,[49] which diverged from its closest relative, *N. gabriellae*, around 0.96 mya. Their geographic distributions are well separated by the Irrawaddy River for eastern and skywalker hoolock gibbons and the Srepok and Ba Rivers for yellow-cheeked crested gibbons. Therefore, we believe they should be designated as a distinct species so as to fully conserve variation. The systematic placement and species validity of all extant gibbons provide critical information for guiding future conservation management strategies.

After reconstructing species-level phylogenetic relationships, we further investigate gene flow occurring during the evolution of gibbons. A previous study has indicated limited introgression between gibbon genera.[9] Hence, we prioritize characterizing interspecific introgression within each genus by D-statistic[50,51] and *f*-branch (f_b) statistics.[52,53] D-statistic quantifies an excess

different colors of the intra-genus nodes in the phylogeny represent the best-fitting model selected for that node based on the Akaike information criterion (AIC) (see STAR Methods and Data S1).

(B) D-statistics for selected species triplets. Each point represents the D-statistic value, and the error bars span three standard deviations (±3 SD) estimated by the weighted block jackknifing over 5 Mb genomic blocks. Values significantly different from zero suggest gene flow between P1 and P3 (if $D > 0$) or P2 and P3 (if $D < 0$). Species in red or blue font highlight pairs with significant D-statistics ($|D| > 0.1$ and $|Z$ score$| > 10$).

(C) Heatmap of f-branch statistics testing for admixture on different branches of the species phylogeny (phylogeny shown at top, and dotted lines are ancestral branches). Warmer colors indicate stronger evidence for admixture involving that branch. Dotted blue lines in the up phylogenetic tree represent ancestral lineages.

See also Figures S2 and S4.

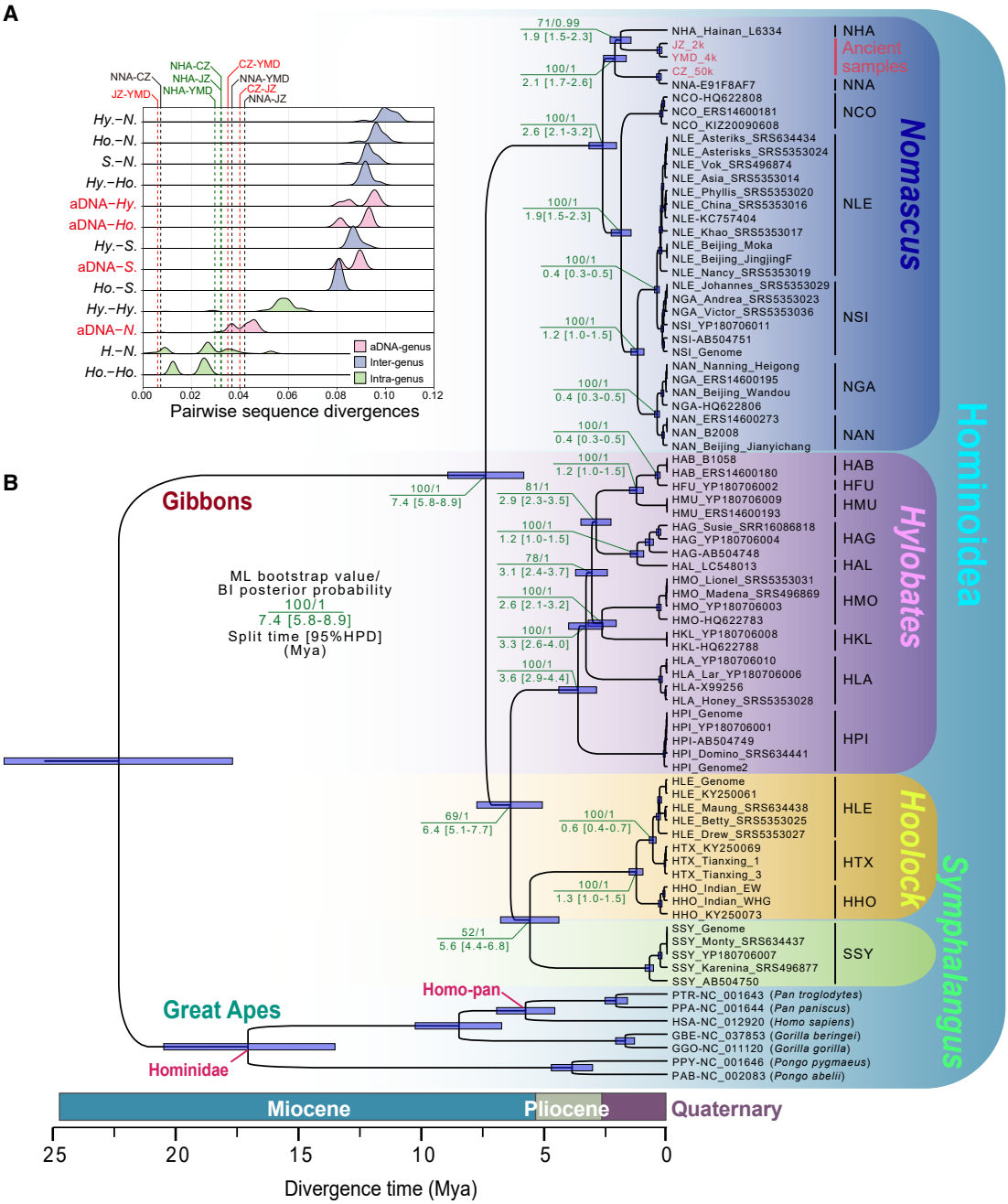

Figure 4. Phylogeny and sequence divergence of mitochondrial genomes of extant and extinct gibbon species

(A) Distribution of pairwise mitochondrial sequence divergences between and within genera. Genus abbreviations are as follows: *Hy.*, *Hylobates*; *Ho.*, *Hoolock*; *N.*, *Nomascus*; *S.*, *Symphalangus*. YMD: ~4,000-year-old gibbon from Yemao Cave, Qijiang District, Chongqing, China. CZ: ~50,000-year-old gibbon from Longlinshan Cave, Manluxincun, Chongzuo, Guangxi Province, China. JZ: *Junzi imperialis* from Shenheyuan tomb (from a ~2,200- to 2,300-year-old tomb possibly belonging to Lady Xia, grandmother of China's first emperor, Qin Shihuang (259–210 BCE), Changan District, Shaanxi Province.

(B) Time tree of extant and extinct gibbon species. The green numbers at the top of the node annotation represent the support values based on the maximum-likelihood (ML) bootstrapping and Bayesian inference (BI) posterior probability. The bottom of node annotations shows split time and the 95% highest posterior density (HPD) interval from the MCMCtree analysis. Two fossil calibrations (Homo-*Pan* and Hominidae) were applied in the MCMCtree algorithm[47] for estimating divergence times.

See also Figure S5.

of derived alleles shared between non-sister taxa and provides statistical evidence of gene flow between *Hy. pileatus* (HPI) and *Hy. lar* (HLA), between *N. concolor* (NCO) and *N. leucogenys* (NLE), between *Hy. moloch* (HMO) and *Hy. agilis* (HAG), and between three gray gibbons: *Hy. muelleri* (HMU), *Hy. abbotti* (HAB), and *Hy. funereus* (HFU) (Figure 3B). The *f*-branch statistic detects gene flow between species on a phylogenetic tree and assigns to specific branches (Figure 3C). Our *f*-branch results corroborate the signals of gene flow detected by D-statistic. The signal between *Hy. moloch* (HMO; endemic to Java Island) and three Bornean gray gibbons (*Hy. muelleri* [HMU], *Hy. abbotti* [HAB], and *Hy. funereus* [HFU]) is surprising given the geographical isolation of these islands. This gene flow suggests historical contact, possibly attributable to land bridges connecting Borneo and Java during glacial periods when sea levels dropped significantly.[54]

Such gene flow caused by natural hybridization highlights that gibbon species can hybridize to produce genetically mixed offspring. Captive breeding programs for gibbon conservation aim to preserve genetically pure lineages, but morphological similarities between some species increase the risk of accidental hybridization without meticulous management and identification. Historically, taxa now recognized as distinct were housed together due to misidentification, posing additional challenges for gibbon conservation breeding. Therefore, we emphasize the necessity of genetic marker-based species identification in managed populations to prevent unwanted hybridization and maintain conservation unit integrity.

DNA phylogeny rectifies the systematic position of extinct gibbons

Fossil evidence[55] and ancient Chinese documentary records[56] suggest that gibbons were historically more widely distributed, particularly in China, extending as far north as the Yellow River. To determine the phylogenetic placement of the three ancient gibbon specimens introduced earlier (JZ_2k, YMD_4k, and CZ_50k), particularly the JZ_2k specimen from the described extinct species *Junzi imperialis*,[5] we analyzed their newly generated mitochondrial genomes alongside those from extant gibbons (Table S5). Pairwise genetic differences (Figure 4A) and phylogenetic trees (Figures 4B, S5C, and S5D) both clearly show that all three specimens cluster within *Nomascus*, specifically with *N. hainanus* and *N. nasutus*. Given the absence of nuclear genomic data, alongside rare genetic introgression[9] and strong reproductive isolation[57] between gibbon genera, our findings imply that *Junzi imperialis* does not constitute a distinct genus. Instead, *J. imperialis* should be reclassified as a species of *Nomascus*. Although two ancient samples (JZ_2k and YMD_4k) cluster with *N. hainanus*, pairwise genetic differences show that they are clearly distinct from this species and refer to potentially a separate species, represented by *J. imperialis*. The CZ_50k gibbon from Chongzuo, Guangxi province, geographically proximates to the historical range of *N. nasutus*, clusters closely with *N. nasutus*, and should be assigned to this species.

Demographic history and genetic diversity of gibbons

Coupling conservation genomics analysis and simulation of habitat distribution enhances our understanding of the vulnerability to extinction. We applied the pairwise sequentially Markovian coalescent (PSMC) model[58] to infer historical fluctuations in effective population size (N_e) across gibbon species using whole-genome sequences (Figures 5A and S6A). To overcome the difficulty of discerning common trends from these individual plots due to differences in absolute N_e scales, we normalized and aggregated the trajectories for all species within each of the four genera (see STAR Methods). This genus-level analysis revealed most gibbon species underwent a bottleneck around ~100–200 kya, followed by a synchronous population recovery until ~70 kya (Figure 5A). We further utilized ecological niche models (ENMs) to reconstruct habitat distribution at this period. These analyses revealed a congruent increase of the ranges of gibbon species from ~100–200 kya to ~70 kya. Coinciding with this pattern, a recession of sea level occurred at the time of ~60–70 kya (Figure 5C), which would lead to an expansion of land and suitable habitat on the Indo-China Peninsula, resulting in increased population sizes of gibbons.

We further examined the genetic diversity patterns of gibbons. Genome-wide heterozygosity revealed significant variation among individuals, with a 10-fold range observed across gibbon species. Heterozygosity ranged from 0.00039 (0.39 heterozygotes per kilobase [kb] pair) in *Ho. hoolock* (HHO) to 0.0041 (4.1 heterozygotes per kb) in *Hy. muelleri* (HMU) (Figures 5D and S6B). The median heterozygosity for all gibbon species was 0.0017. Notably, *Hoolock* species, including *Ho. hoolock*, *Ho. leuconedys* (HLE), and *Ho. tianxing* (HTX), exhibited the lowest heterozygosity values. By contrast, three species from Borneo, *Hy. funereus* (HFU), *Hy. abbotti* (HAB), and *Hy. muelleri* (HMU), show the highest heterozygosity (2.9–3.7 heterozygotes per kb).[60]

To investigate more recent demographic events, particularly potential inbreeding that PSMC analyses may not fully capture, we further analyzed runs of homozygosity (RoHs) in different gibbon species. RoH is a widely recognized method for quantifying recent inbreeding and genomic erosion resulting from contemporary population declines. We focused on the number of RoHs and the fraction of the genome in RoHs, considering a minimum RoH length of $\geq$1 Mbp, and compared these values with those of great apes (Figures 5E and S6C).[60] The species-wide median genome fraction in RoHs is 4.0%, and the median number of RoHs is 45. Among 17 gibbon species (except the low genomic coverage of Hainan gibbon), *Hy. pileatus* (HPI) has the largest number of RoHs and the largest genome fraction in RoHs, followed by the three *Hoolock* species. Compared with great apes, these two parameters are between those of the critically endangered eastern gorilla (*Gorilla beringei* [GBE]) and other great apes. This suggests that these four species have undergone high levels of recent inbreeding. In particular, one *Ho. hoolock* and one *Ho. leuconedys* individual show significant inbreeding with over 340 RoHs and 45% of the genome in RoHs (Figures 5E and S6C). All these genetics parameters, including low heterozygosity and high levels of RoHs, demonstrate that *Hoolock* species have experienced a serious population decline, which has likely resulted in increased levels of population inbreeding. These findings underscore the need for conservation efforts that take these genetic parameters into account. However, some critically endangered gibbon species,

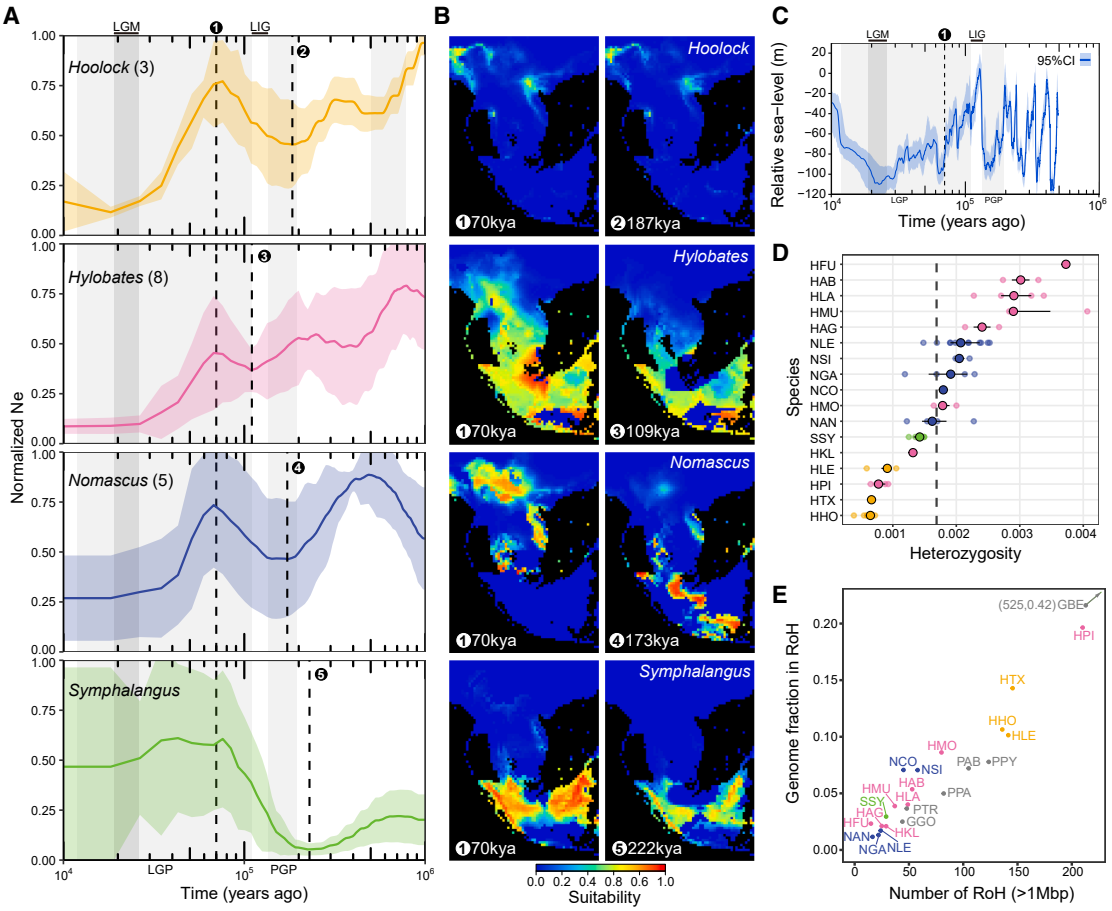

Figure 5. Demographic history and genetic diversity of gibbons

(A) Genus-level normalized historical effective population size (N_e) trajectories inferred from PSMC results. To reveal common trends, the N_e trajectory of each species was normalized by dividing it by that species's maximum N_e value observed across the entire time period. This panel shows the mean (bold colored line) and standard deviation (shaded area) of all normalized species trajectories within each genus. Species numbers per genus are given in parentheses, with *Symphalangus* represented by its single species (four individuals). Gray shaded vertical bars: the last interglacial (LIG, ~115–135 kya), the Last Glacial Period (LGP, ~12–110 kya), the Last Glacial Maximum (LGM, ~19–26 kya), and the Penultimate Glacial Period (PGP, ~135–194 kya). Generation time (g = 15 years) and mutation rate ($\mu = 1.0 \times 10^{-8}$ per site per generation) are used for scaling axes.

(B) Ecological niche model (ENM) reconstructions of suitable habitats for each genus at key demographic time points (indicated by circled numbers in A). The maps show predicted habitat suitability (from low in blue to high in red), illustrating the expansion of suitable habitats from ~100–200 to ~70 kya.

(C) Relative sea level during the time period between 10 and 500 kya.[59] A local minimum in relative sea level is observed around 60–70 kya, preceding the LGM.

(D) Heterozygosity across the 17 gibbon species. Solid circles and whiskers represent the median and interquartile range. The gray dashed line denotes the median heterozygosity across all individuals.

(E) Median number of RoHs vs. median genome fraction of RoHs per species. Species abbreviations are as in Table 1. Great ape species are included for comparison[60]: PPA, *Pan paniscus*; PTR, *Pan troglodytes*; GBE, *Gorilla beringei*; GGO, *Gorilla gorilla*; PAB, *Pongo abelii*; PPY, *Pongo pygmaeus*.

See also Figure S6.

such as *N. concolor* (NCO), *N. siki* (NSI), and *N. leucogenys* (NLE), exhibit relatively lower numbers and shorter total lengths of RoHs compared with some less threatened species or even the highly inbred *Hoolock* species (Figures 5E and S5C). This observation suggests that while high levels of RoH can indicate recent bottlenecks or intense inbreeding that may increase vulnerability, RoH alone is an insufficient predictor of extinction risk. Extinction risk is a complex outcome influenced by long-term demographic history, current population size, habitat status, and specific threats, which may not always be reflected by a single parameter.

Comparative genomics identifies a functional SV associated with limb lengthening in gibbons

As an adaptation to their unique locomotion behavior, gibbons have evolved long arms and legs. Some candidate genes that have evolved rapidly due to single-nucleotide mutations in the gibbon lineage and which might be associated with the evolution of long limbs have been previously reported.[8,24,61] Here, we shift our attention from single-nucleotide mutations to structural variants (SVs), which are large genomic alterations typically defined as encompassing at least 50 bp, including deletions, duplications, insertions, inversions, and translocations. These variants have

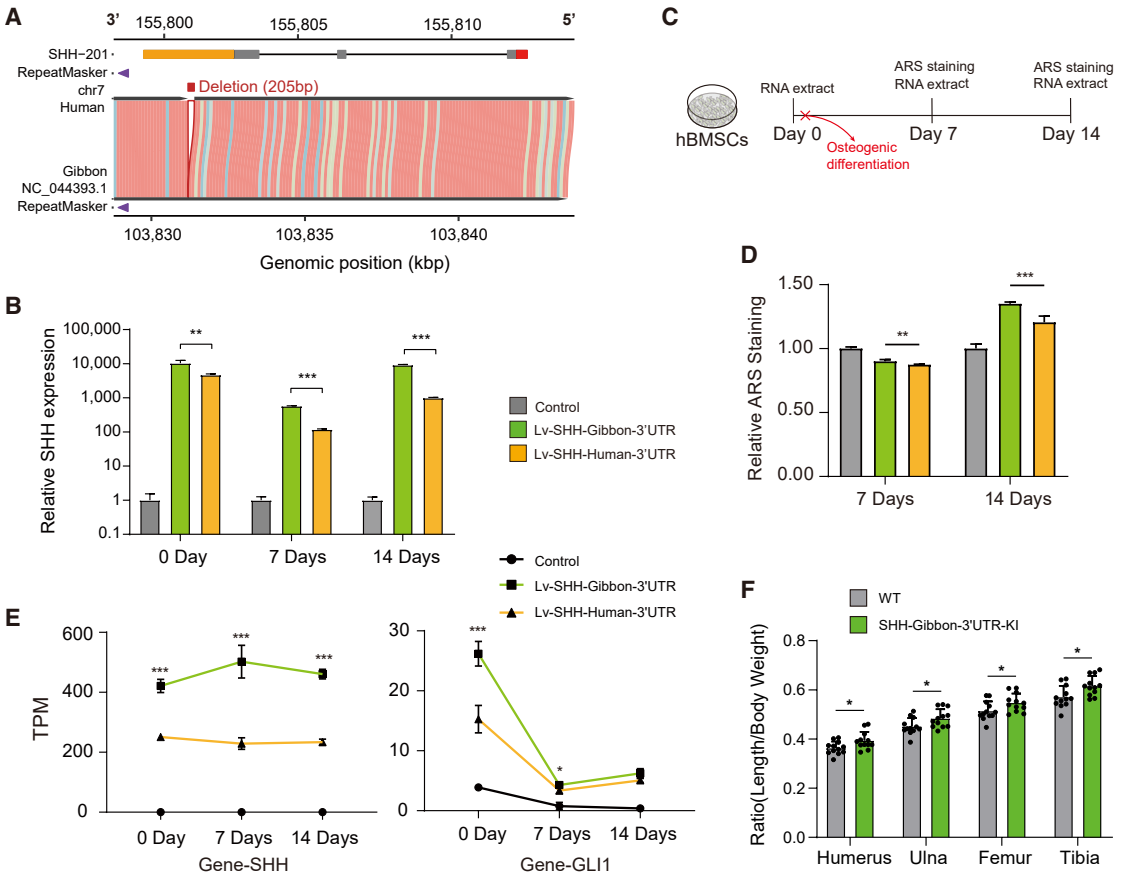

Figure 6. Multi-level experiments to study the functional significance of the gibbon-specific deletion (chr7:155801422–155801627, hg38) in the 3′ UTR of the *SHH* gene

(A) Genomic context of the 205 bp deletion in the *SHH* 3′ UTR. The top track shows the human *SHH* gene structure (isoform SHH-201). The bottom tracks show a sequence alignment of the human and a representative gibbon genome (NSI), highlighting the precise location of the gibbon-specific deletion. RepeatMasker annotations are also shown.

(B) Relative expression levels of *SHH* in human bone marrow mesenchymal stem cells (hBMSCs) transduced with lentiviral vectors containing either the human or gibbon 3′ UTR. qPCR analyses were performed at days 0, 7, and 14 of osteogenic differentiation.

(C) Schematic of *in vitro* osteogenic differentiation experiment in hBMSCs, and the time points for alizarin red S (ARS) staining and RNA extraction.

(D) ARS staining reveals that hBMSCs overexpressing *SHH* with the gibbon 3′ UTR display a higher ability of calcium mineralization than hBMSCs with the human 3′ UTR ($p = 0.0017$ after 7 days and $p = 3.4E{-}5$ after 14 days).

(E) RNA sequencing data show significantly higher expression levels (transcripts per million [TPM]) of *SHH* (left) and its key downstream target *GLI1* (right) in cell lines expressing *SHH* with gibbon 3′ UTR compared with those with human 3′ UTR after 7 and 14 days after osteogenic differentiation of hBMSCs.

(F) Relative limb bone lengths (normalized by body weight) in wild-type (WT) and homozygous gibbon-SHH-3′ UTR knockin (KI) mice. All four measured bones show a significant increase in relative length in KI mice.

Data in bar charts and line plots are presented as mean ± SEM. Statistical significance was determined by Student's *t* test (for B and D–G). ns, not significant; * $p < 0.05$, ** $p < 0.01$, *** $p < 0.001$.

See also Figure S7.

been shown to play a significant role in phenotypic evolution and human diseases.[62,63] Recent advancements in sequencing technology and bioinformatics have enabled significant progress in mapping these variants and interpreting their functional impacts.[63,64] Through whole-genome alignment, we identified 69,202 deletions and 72,262 insertions in gibbons compared with the human genome. Subsequently, by focusing on gibbon-specific SVs (Table S8) occurring at those genes associated with mammalian limb length phenotypes (from the MGI database[65]) (Table S9), we narrowed this list to 22 high-priority candidates (Table S10). Among these, a 205 bp deletion (chromosome 7 [chr7]:155801422–155801627, hg38) within the 3′ untranslated region (3′ UTR) of the *SHH* gene was of particular interest (Figure 6A), given SHH's critical role in limb evolution and development.[66–68] A luciferase reporter assay in human bone marrow mesenchymal stem cells (hBMSCs) and 293T cells indicated that the gibbon 3′ UTR sequence significantly increased reporter expression compared with the human 3′ UTR sequences (Figure S7A).

To further disentangle the functional role of this deletion, we constructed lentiviral vectors containing either human or gibbon-*SHH* 3′ UTR sequences and transduced them into

hBMSCs. Quantitative PCR (qPCR) analysis supported that the gibbon 3′ UTR variant led to significantly higher *SHH* expression levels compared with the human variant (Figure 6B; $p < 0.01$). We then performed osteogenic differentiation of the transduced hBMSCs and used alizarin red S (ARS) staining to determine calcium nodule formation in the different cell lines at 7 and 14 days after differentiation, respectively (Figure 6C). ARS staining revealed that hBMSCs overexpressing *SHH* with the gibbon 3′ UTR sequence exhibited significantly enhanced calcium mineralization compared with those expressing the human 3′ UTR (Figure 6D; $p = 0.0017$ at 7 days and $p = 3.4 \times 10^{-5}$ at 14 days). We further identified differentially expressed genes (DEGs) between two cell lines at different time points (Figure S7B). As expected, and validated by qPCR, *SHH* expression was consistently higher in cell lines carrying the gibbon 3′ UTR sequence compared with the human variant at both 7 and 14 days (Figures 6B and 6E). Additionally, *GLI1* (GLI family zinc-finger 1), a key component of the Hedgehog/GLI signaling pathway crucial for limb development,[66–68] was significantly upregulated in cells with the gibbon 3′ UTR at day 0 (Figure 6E). Gene enrichment analysis of these DEGs revealed categories, including extracellular matrix organization (Figure S7D), that are involved in regulating cell adhesion, proliferation, and responses to growth factors, differentiation, and ultimately, the functional characteristics of bone.[69]

Finally, we generated knockin (KI) mice by inserting the gibbon 3′ UTR sequence after the termination codon of the mouse *SHH*. Using microcomputed tomography (micro-CT), we measured bone lengths (humerus, ulna, femur, and tibia) in wild-type and gibbon-*SHH* homozygous KI mice (Figure S7E; Table S11). Results demonstrated significantly longer relative limbs in the gibbon-*SHH* KI mice compared with controls (Figures 6F and S7F). Quantitatively, transgenic mice exhibited an average increase in relative limb length of 7.44% (normalized by weight), with a large standardized effect size (average Cohen's d = 0.95). The percentage increases in relative limb length were relatively uniform across all limb segments (ranging from 6.4% to 8.3%). The finding provides *in vivo* evidence that the gibbon-specific deletion contributes to limb elongation. To explore the broader relevance of this finding, we investigated whether variation at the human *SHH* locus is similarly associated with limb phenotypes. A comprehensive search of human genome-wide association study (GWAS) catalogs[70–73] and SV databases[74,75] yielded no significant association between common variants at the *SHH* locus and limb length, nor did we find any analogous deletions in the human *SHH* 3′ UTR. These data suggest that the 205 bp deletion is a gibbon-specific evolutionary innovation as a genetic basis for their characteristic limb elongation.

DISCUSSION

Gibbons or small apes are a neglected group of primates in the shadow of the great apes. Our knowledge about this primate group is insufficient, and fundamental information, such as their adaptability and evolutionary history, is still missing. In this study, we present large-scale genome data for 18 gibbon species and mitochondrial genomes of 3 ancient samples. We settled the disputed phylogeny of the four gibbon genera using whole-genome alignment data from four *de novo* assemblies. The large ancient population sizes and rapid speciation of gibbons play a significant role in the discordant phylogenetic relationships among the four genera. We further reconstructed phylogenetic trees and confirmed all currently recognized gibbon species as valid, which is the basis for proper conservation management. For the ancient specimens, we show that all of them belong to the genus *Nomascus*, and one of them refers to the extant *N. nasutus* and two of them to the extinct *Nomascus imperialis*. Further, we integrate conservation genomics analysis and ecological niche modeling to reveal the roles of climate change and human activities on the population dynamics of gibbons over the last ~120,000 years. Finally, we identified a SV at the *SHH* gene that likely contributes to long limb formation in gibbons. In conclusion, this study expands our knowledge of the mechanisms underlying the evolution and adaptability of gibbons, paving the way for future investigation of this unique primate clade in many fields of research.

Limitations of the study

While this study provides valuable insights into gibbon phylogeny and evolution, several limitations should be considered. First, while our genomic analysis encompassed 18 gibbon species, we notably lack nuclear genomic data for 2 extant species (eastern black-crested, *N. nasutus*; and Bornean white-bearded gibbons, *Hy. albibarbis*) and high-coverage genomic data for the Hainan gibbon, primarily due to challenges in obtaining high-quality samples suitable for whole-genome sequencing for these rare and elusive species, potentially missing key evolutionary insights. Second, our ancient DNA analysis, restricted to mitochondrial genomes from three specimens, provides only maternal lineage information and precludes comprehensive historical genomic insights. Furthermore, the limited number of samples per species constrains our ability to reconstruct recent population histories, particularly during periods of intensive human activity in Southeast and South Asia. This sampling limitation prevents robust estimation of anthropogenic impacts on gibbon population dynamics, highlighting the need for more extensive population-level sampling in future studies. Nevertheless, our comprehensive genomic analyses have illuminated gibbon phylogeny, demographic history, and conservation status, establishing a robust foundation for future investigations into primate evolution and conservation.

RESOURCE AVAILABILITY

Lead contact

Further information and requests for resources and reagents should be directed to and will be fulfilled by the lead contact, Dong-Dong Wu (wudongdong@mail.kiz.ac.cn).

Materials availability

No new unique reagents were generated in this study.

Data and code availability

The gibbon genome assemblies and the raw short-read sequencing data have been deposited at the China National Center for Bioinformation under BioProject accession no. PRJCA035014. All genome annotation GFF files have been uploaded to the public Mendeley Data (https://doi.org/10.17632/j386wp59tt.1). Mitochondrial DNA sequences (FASTA format) have been deposited at the GenBase[76] in the National Genomics Data Center[77] under BioProject accession no. PRJCA028505. The code used to run heterozygosity and RoH on the resequencing individuals is available on GitHub

(https://github.com/shengwang/snakemake-primates-cg). Any additional information required to reanalyze the data reported in this paper is available from the lead contact upon request.

ACKNOWLEDGMENTS

We thank the staff members of the National Research Facility for Phenotypic & Genetic Analysis of Model Animals (Primate Facility) (https://cstr.cn/31137.02.NPRC) for providing technical support and assistance in data collection and analysis. This study was supported by the National Key Research and Development Program (no. 2022YFF1301500), the National Natural Science Foundation of China (nos. 41925009 and 32100489), the Chinese Academy of Sciences (CAS) "Light of West China" Program (XBZG-ZDSYS-202213), the Chinese Academy of Sciences (CAS) (YSBR-019), the Youth Innovation Promotion Association CAS, the Yunnan Provincial Department of Science and Technology (202305AH340006), the Yunnan Revitalization Talent Support Program Yunling Scholar Project, and the Yunnan Revitalization Talent Support Program Young Talent Project.

AUTHOR CONTRIBUTIONS

Conceptualization, D.-D.W., Q.F., and P.F.; formal analysis, S.W., Z.C., A.L., X.Y., and X.T.; code development, S.W., Z.C., A.L., X.Y., and X.T.; visualization, S.W., Z.C., A.L., X.Y., and X.T.; investigation, X.Y., Y.Z., F.L., Q.D., X.F., Y.P., and M.Z.; funding acquisition, D.-D.W., Q.F., P.F., S.W., and Z.C.; project administration, D.-D.W., Q.F., P.F., and S.W.; resources, A.C.K., M.T., G.U., S.H., T.Z., Y.D., L.L., and C.R.; writing – original draft, S.W. and D.-D.W.; writing – review and editing, D.-D.W., Q.F., P.F., S.W., Z.C., A.L., A.C.K., X.T., and C.R.; supervision, D.-D.W., Q.F., and P.F.

DECLARATION OF INTERESTS

The authors declare no competing interests.

STAR★METHODS

Detailed methods are provided in the online version of this paper and include the following:

- KEY RESOURCES TABLE
- EXPERIMENTAL MODEL AND STUDY PARTICIPANT DETAILS
  - Generating stable transfection cells
  - Generating CRISPR/Cas9 mice
- METHOD DETAILS
  - Genome scaffolding and annotation
  - Genome re-sequencing dataset collection and processing
  - Phylogeny and incomplete lineage sorting across four gibbon genera
  - Phylogeny and gene flow among three gibbon genera
  - Phylogenetic analysis using ancient and extant gibbon mitochondrial DNA
  - Population history and genetic diversity analysis
  - Ecological niche modeling
  - Structural variant (SV) calling, genotyping and annotation
  - Experiments to study the functional consequences of the structural variant in the SHH gene

SUPPLEMENTAL INFORMATION

Supplemental information can be found online at https://doi.org/10.1016/j.cell.2025.10.016.

Received: January 21, 2025
Revised: July 2, 2025
Accepted: October 15, 2025
Published: November 7, 2025

REFERENCES

1. Williamson, E., Maisels, F., Groves, C., Fruth, B., Humle, T., and Morton, F. (2013). Handbook of the Mammals of the World, Volume 3: Primates (Lynx Edicions).
2. IUCN (2024). The IUCN Red List of Threatened Species. Version 2024-1 (International Union for Conservation of Nature [IUCN]).
3. Michilsens, F., Vereecke, E.E., D'Août, K., and Aerts, P. (2009). Functional anatomy of the gibbon forelimb: adaptations to a brachiating lifestyle. J. Anat. *215*, 335–354. https://doi.org/10.1111/j.1469-7580.2009.01109.x.
4. Ortiz, A., Pilbrow, V., Villamil, C.I., Korsgaard, J.G., Bailey, S.E., and Harrison, T. (2015). The Taxonomic and Phylogenetic Affinities of Bunopithecus sericus, a Fossil Hylobatid from the Pleistocene of China. PLoS One *10*, e0131206. https://doi.org/10.1371/journal.pone.0131206.
5. Turvey, S.T., Bruun, K., Ortiz, A., Hansford, J., Hu, S.M., Ding, Y., Zhang, T.E., and Chatterjee, H.J. (2018). New genus of extinct Holocene gibbon associated with humans in Imperial, China. Science *360*, 1346–1349. https://doi.org/10.1126/science.aao4903.
6. Ding, Y. (2009). Identifying the owner of the Shenheyuan Warring States period tomb of the Qin State. Kaogu Yu Wenwu *2009*, 62–66.
7. Hu, S., Yang, T., Yang, M., Ding, Y., Cai, D., and Zhang, T.e. (2023). The Zooarchaeological Research of Animal Remains from the Burial Pit K12 of the Warring States Period Qin Mausoleum at Shenheyuan in Chang'an, Shaanxi. Acta Archaeol. Sinica *1*, 123–148.
8. Carbone, L., Harris, R.A., Gnerre, S., Veeramah, K.R., Lorente-Galdos, B., Huddleston, J., Meyer, T.J., Herrero, J., Roos, C., Aken, B., et al. (2014). Gibbon genome and the fast karyotype evolution of small apes. Nature *513*, 195–201. https://doi.org/10.1038/nature13679.
9. Shi, C.M., and Yang, Z.H. (2018). Coalescent-Based Analyses of Genomic Sequence Data Provide a Robust Resolution of Phylogenetic Relationships among Major Groups of Gibbons. Mol. Biol. Evol. *35*, 159–179. https://doi.org/10.1093/molbev/msx277.
10. Veeramah, K.R., Woerner, A.E., Johnstone, L., Gut, I., Gut, M., Marques-Bonet, T., Carbone, L., Wall, J.D., and Hammer, M.F. (2015). Examining Phylogenetic Relationships Among Gibbon Genera Using Whole Genome Sequence Data Using an Approximate Bayesian Computation Approach. Genetics *200*, 295–308. https://doi.org/10.1534/genetics.115.174425.
11. Geissmann, T. (2002). Taxonomy and evolution of gibbons. Evol. Anthropol. *11*, 28–31. https://doi.org/10.1002/evan.10047.
12. Müller, S., Hollatz, M., and Wienberg, J. (2003). Chromosomal phylogeny and evolution of gibbons (Hylobatidae). Hum. Genet. *113*, 493–501. https://doi.org/10.1007/s00439-003-0997-2.
13. Israfil, H., Zehr, S.M., Mootnick, A.R., Ruvolo, M., and Steiper, M.E. (2011). Unresolved molecular phylogenies of gibbons and siamangs (Family: Hylobatidae) based on mitochondrial, Y-linked, and X-linked loci indicate a rapid Miocene radiation or sudden vicariance event. Mol. Phylogenet. Evol. *58*, 447–455. https://doi.org/10.1016/j.ympev.2010.11.005.
14. Meyer, T.J., McLain, A.T., Oldenburg, J.M., Faulk, C., Bourgeois, M.G., Conlin, E.M., Mootnick, A.R., de Jong, P.J., Roos, C., Carbone, L., et al. (2012). An Alu-Based Phylogeny of Gibbons (Hylobatidae). Mol. Biol. Evol. *29*, 3441–3450. https://doi.org/10.1093/molbev/mss149.
15. Chan, Y.C., Roos, C., Inoue-Murayama, M., Inoue, E., Shih, C.C., and Vigilant, L. (2012). A comparative analysis of Y chromosome and mtDNA phylogenies of the Hylobates gibbons. BMC Evol. Biol. *12*, 150. https://doi.org/10.1186/1471-2148-12-150.
16. Wall, J.D., Kim, S.K., Luca, F., Carbone, L., Mootnick, A.R., de Jong, P.J., and Di Rienzo, A. (2013). Incomplete Lineage Sorting Is Common in Extant Gibbon Genera. PLoS One *8*, e53682. https://doi.org/10.1371/journal.pone.0053682.

17. Rivas-González, I., Rousselle, M., Li, F., Zhou, L., Dutheil, J.Y., Munch, K., Shao, Y., Wu, D., Schierup, M.H., and Zhang, G. (2023). Pervasive incomplete lineage sorting illuminates speciation and selection in primates. Science *380*, eabn4409. https://doi.org/10.1126/science.abn4409.

18. Thinh, V.N., Mootnick, A.R., Geissmann, T., Li, M., Ziegler, T., Agil, M., Moisson, P., Nadler, T., Walter, L., and Roos, C. (2010). Mitochondrial evidence for multiple radiations in the evolutionary history of small apes. BMC Evol. Biol. *10*, 74. https://doi.org/10.1186/1471-2148-10-74.

19. Aung, P.P., Lwin, N., Aung, T.H., Htike, T.S.M., Thompson, C., Roos, C., Zaw, S.M., Lum, L.Z., Oo, W.N., Sau, Z., et al. (2024). Confirmation of Skywalker Hoolock Gibbon (Hoolock tianxing) in Myanmar Extends Known Geographic Range of an Endangered Primate. Int. J. Primatol. *45*, 810–833. https://doi.org/10.1007/s10764-024-00418-6.

20. Li, B.-G., Zhang, H., Li, M., Jiang, X.-L., Fan, P.-F., Zhou, J., Guo, S.-T., Qi, X.-G., Li, J.-H., Lu, J.-Q., et al. (2024). Achievements and challenges of primate conservation in China. Zool. Res.: Divers. Conserv. *1*, 66–74. https://doi.org/10.24272/j.issn.2097-3772.2023.298.

21. Li, B.-G. (2022). Assessment Report on the Endangered Status of Primates in China. 40th Anniversary of the Establishment of the National Scientific Committee on Endangered Species and 2022 Annual Conference (in Chinese).

22. Estrada, A., Garber, P.A., Rylands, A.B., Roos, C., Fernandez-Duque, E., Di Fiore, A., Nekaris, K.A.-I., Nijman, V., Heymann, E.W., Lambert, J.E., et al. (2017). Impending extinction crisis of the world's primates: Why primates matter. Sci. Adv. *3*, e1600946. https://doi.org/10.1126/sciadv.1600946.

23. Zhao, X., Garber, P.A., Ye, X., and Li, M. (2023). The impact of climate change and human activities over the past 2000 years has increased the spatial-temporal extinction rate of gibbons. Biol. Conserv. *281*, 109998. https://doi.org/10.1016/j.biocon.2023.109998.

24. Shao, Y., Zhou, L., Li, F., Zhao, L., Zhang, B.-L., Shao, F., Chen, J.-W., Chen, C.-Y., Bi, X., Zhuang, X.-L., et al. (2023). Phylogenomic analyses provide insights into primate evolution. Science *380*, 913–924. https://doi.org/10.1126/science.abn6919.

25. Wu, D.-D., Qi, X.-G., Yu, L., Li, M., Liu, Z.-J., Yoder, A.D., Roos, C., Hayakawa, T., Rogers, J., Marques-Bonet, T., et al. (2022). Initiation of the Primate Genome Project. Zool. Res. *43*, 147–149. https://doi.org/10.24272/j.issn.2095-8137.2022.001.

26. Lieberman-Aiden, E., van Berkum, N.L., Williams, L., Imakaev, M., Ragoczy, T., Telling, A., Amit, I., Lajoie, B.R., Sabo, P.J., Dorschner, M. O., et al. (2009). Comprehensive Mapping of Long-Range Interactions Reveals Folding Principles of the Human Genome. Science *326*, 289–293. https://doi.org/10.1126/science.1181369.

27. Burton, J.N., Adey, A., Patwardhan, R.P., Qiu, R., Kitzman, J.O., and Shendure, J. (2013). Chromosome-scale scaffolding of de novo genome assemblies based on chromatin interactions. Nat. Biotechnol. *31*, 1119–1125. https://doi.org/10.1038/nbt.2727.

28. Alonge, M., Lebeigle, L., Kirsche, M., Jenike, K., Ou, S., Aganezov, S., Wang, X., Lippman, Z.B., Schatz, M.C., and Soyk, S. (2022). Automated assembly scaffolding using RagTag elevates a new tomato system for high-throughput genome editing. Genome Biol. *23*, 258. https://doi.org/10.1186/s13059-022-02823-7.

29. Birney, E., Clamp, M., and Durbin, R. (2004). GeneWise and genomewise. Genome Res. *14*, 988–995. https://doi.org/10.1101/gr.1865504.

30. Stanke, M., Keller, O., Gunduz, I., Hayes, A., Waack, S., and Morgenstern, B. (2006). AUGUSTUS: ab initio prediction of alternative transcripts. Nucleic Acids Res. *34*, W435–W439. https://doi.org/10.1093/nar/gkl200.

31. Charlesworth, D. (2017). Evolution of recombination rates between sex chromosomes. Philos. Trans. R. Soc. Lond. B Biol. Sci. *372*, 20160456. https://doi.org/10.1098/rstb.2016.0456.

32. Makova, K.D., Pickett, B.D., Harris, R.S., Hartley, G.A., Cechova, M., Pal, K., Nurk, S., Yoo, D., Li, Q., Hebbar, P., et al. (2024). The complete sequence and comparative analysis of ape sex chromosomes. Nature *630*, 401–411. https://doi.org/10.1038/s41586-024-07473-2.

33. Haimoff, E.H., Chivers, D.J., Gittins, S.P., and Whitten, T. (1982). A phylogeny of gibbons (Hylobates spp.) based on morphological and behavioural characters. Folia Primatol. (Basel) *39*, 213–237. https://doi.org/10.1159/000156079.

34. Degnan, J.H., and Rosenberg, N.A. (2009). Gene tree discordance, phylogenetic inference and the multispecies coalescent. Trends Ecol. Evol. *24*, 332–340. https://doi.org/10.1016/j.tree.2009.01.009.

35. Pamilo, P., and Nei, M. (1988). Relationships between gene trees and species trees. Mol. Biol. Evol. *5*, 568–583. https://doi.org/10.1093/oxfordjournals.molbev.a040517.

36. Valiente-Mullor, C., Beamud, B., Ansari, I., Francés-Cuesta, C., García-González, N., Mejía, L., Ruiz-Hueso, P., and González-Candelas, F. (2021). One is not enough: On the effects of reference genome for the mapping and subsequent analyses of short-reads. PLoS Comput. Biol. *17*, e1008678. https://doi.org/10.1371/journal.pcbi.1008678.

37. Prasad, A., Lorenzen, E.D., and Westbury, M.V. (2022). Evaluating the role of reference-genome phylogenetic distance on evolutionary inference. Mol. Ecol. Resour. *22*, 45–55. https://doi.org/10.1111/1755-0998.13457.

38. Yang, X., Lee, W.P., Ye, K., and Lee, C. (2019). One reference genome is not enough. Genome Biol. *20*, 104. https://doi.org/10.1186/s13059-019-1717-0.

39. Degnan, J.H., and Rosenberg, N.A. (2006). Discordance of Species Trees with Their Most Likely Gene Trees. PLoS Genet. *2*, e68. https://doi.org/10.1371/journal.pgen.0020068.

40. Liu, L., and Edwards, S.V. (2009). Phylogenetic Analysis in the Anomaly Zone. Syst. Biol. *58*, 452–460. https://doi.org/10.1093/sysbio/syp034.

41. Mendes, F.K., and Hahn, M.W. (2018). Why Concatenation Fails Near the Anomaly Zone. Syst. Biol. *67*, 158–169. https://doi.org/10.1093/sysbio/syx063.

42. Rannala, B., and Yang, Z. (2017). Efficient Bayesian Species Tree Inference under the Multispecies Coalescent. Syst. Biol. *66*, 823–842. https://doi.org/10.1093/sysbio/syw119.

43. Dutheil, J.Y., Ganapathy, G., Hobolth, A., Mailund, T., Uyenoyama, M.K., and Schierup, M.H. (2009). Ancestral Population Genomics: The Coalescent Hidden Markov Model Approach. Genetics *183*, 259–274. https://doi.org/10.1534/genetics.109.103010.

44. Chan, Y.C., Roos, C., Inoue-Murayama, M., Inoue, E., Shih, C.C., Pei, K. J.C., and Vigilant, L. (2013). Inferring the evolutionary histories of divergences in Hylobates and Nomascus gibbons through multilocus sequence data. BMC Evol. Biol. *13*, 82. https://doi.org/10.1186/1471-2148-13-82.

45. Prado-Martinez, J., Sudmant, P.H., Kidd, J.M., Li, H., Kelley, J.L., Lorente-Galdos, B., Veeramah, K.R., Woerner, A.E., O'Connor, T.D., Santpere, G., et al. (2013). Great ape genetic diversity and population history. Nature *499*, 471–475. https://doi.org/10.1038/nature12228.

46. Mailund, T., Munch, K., and Schierup, M.H. (2014). Lineage sorting in apes. Annu. Rev. Genet. *48*, 519–535. https://doi.org/10.1146/annurev-genet-120213-092532.

47. Yang, Z., and Rannala, B. (2006). Bayesian Estimation of Species Divergence Times Under a Molecular Clock Using Multiple Fossil Calibrations with Soft Bounds. Mol. Biol. Evol. *23*, 212–226. https://doi.org/10.1093/molbev/msj024.

48. Fan, P.F., He, K., Chen, X., Ortiz, A., Zhang, B., Zhao, C., Li, Y.Q., Zhang, H.B., Kimock, C., Wang, W.Z., et al. (2017). Description of a new species of Hoolock gibbon (Primates: Hylobatidae) based on integrative taxonomy. Am. J. Primatol. *79*, e22631. https://doi.org/10.1002/ajp.22631.

49. Thinh, V.N., Mootnick, A.R., Thanh, V.N., Nadler, T., and Roos, C. (2010). A new species of crested gibbon, from the central Annamite mountain range. Viet. J. Primatol. *4*, 1–12.

50. Green, R.E., Krause, J., Briggs, A.W., Maricic, T., Stenzel, U., Kircher, M., Patterson, N., Li, H., Zhai, W., Fritz, M.H.Y., et al. (2010). A draft sequence of the Neandertal genome. Science *328*, 710–722. https://doi.org/10.1126/science.1188021.

51. Durand, E.Y., Patterson, N., Reich, D., and Slatkin, M. (2011). Testing for Ancient Admixture between Closely Related Populations. Mol. Biol. Evol. *28*, 2239–2252. https://doi.org/10.1093/molbev/msr048.

52. Malinsky, M., Matschiner, M., and Svardal, H. (2021). Dsuite - Fast D-statistics and related admixture evidence from VCF files. Mol. Ecol. Resour. *21*, 584–595. https://doi.org/10.1111/1755-0998.13265.

53. Malinsky, M., Svardal, H., Tyers, A.M., Miska, E.A., Genner, M.J., Turner, G.F., and Durbin, R. (2018). Whole-genome sequences of Malawi cichlids reveal multiple radiations interconnected by gene flow. Nat. Ecol. Evol. *2*, 1940–1955. https://doi.org/10.1038/s41559-018-0717-x.

54. Bird, M.I., Taylor, D., and Hunt, C. (2005). Palaeoenvironments of insular Southeast Asia during the Last Glacial Period: a savanna corridor in Sundaland? Quat. Sci. Rev. *24*, 2228–2242. https://doi.org/10.1016/j.quascirev.2005.04.004.

55. Jablonski, N.G., and Chaplin, G. (2009). The Fossil Record of Gibbons. In The Gibbons. Developments in Primatology: Progress and Prospects, D. Whittaker and S. Lappan, eds. (Springer), pp. 111–130. https://doi.org/10.1007/978-0-387-88604-6_7.

56. van Gulik, R.H. (1967). The Gibbon in China: an Essay in Chinese Animal Lore (E.J. Brill).

57. Myers, R.H., and Shafer, D.A. (1979). Hybrid Ape Offspring of a Mating of Gibbon and Siamang. Science *205*, 308–310. https://doi.org/10.1126/science.451603.

58. Li, H., and Durbin, R. (2011). Inference of human population history from individual whole-genome sequences. Nature *475*, 493–496. https://doi.org/10.1038/nature10231.

59. Grant, K.M., Rohling, E.J., Ramsey, C.B., Cheng, H., Edwards, R.L., Florindo, F., Heslop, D., Marra, F., Roberts, A.P., Tamisiea, M.E., et al. (2014). Sea-level variability over five glacial cycles. Nat. Commun. *5*, 5076. https://doi.org/10.1038/ncomms6076.

60. Kuderna, L.F.K., Gao, H., Janiak, M.C., Kuhlwilm, M., Orkin, J.D., Bataillon, T., Manu, S., Valenzuela, A., Bergman, J., Rousselle, M., et al. (2023). A global catalog of whole-genome diversity from 233 primate species. Science *380*, 906–913. https://doi.org/10.1126/science.abn7829.

61. Bi, X., Zhou, L., Zhang, J.-J., Feng, S., Hu, M., Cooper, D.N., Lin, J., Li, J., Wu, D.-D., and Zhang, G. (2023). Lineage-specific accelerated sequences underlying primate evolution. Sci. Adv. *9*, eadc9507. https://doi.org/10.1126/sciadv.adc9507.

62. Ho, S.S., Urban, A.E., and Mills, R.E. (2020). Structural variation in the sequencing era. Nat. Rev. Genet. *21*, 171–189. https://doi.org/10.1038/s41576-019-0180-9.

63. Weischenfeldt, J., Symmons, O., Spitz, F., and Korbel, J.O. (2013). Phenotypic impact of genomic structural variation: insights from and for human disease. Nat. Rev. Genet. *14*, 125–138. https://doi.org/10.1038/nrg3373.

64. Spielmann, M., Lupiáñez, D.G., and Mundlos, S. (2018). Structural variation in the 3D genome. Nat. Rev. Genet. *19*, 453–467. https://doi.org/10.1038/s41576-018-0007-0.

65. Baldarelli, R.M., Smith, C.L., Ringwald, M., Richardson, J.E., and Bult, C. J.; Mouse Genome Informatics Group (2024). Mouse Genome Informatics: an integrated knowledgebase system for the laboratory mouse. Genetics *227*, iyae031. https://doi.org/10.1093/genetics/iyae031.

66. Tickle, C., and Towers, M. (2017). Sonic Hedgehog Signaling in Limb Development. Front. Cell Dev. Biol. *5*, 14. https://doi.org/10.3389/fcell.2017.00014.

67. Petit, F., Sears, K.E., and Ahituv, N. (2017). Limb development: a paradigm of gene regulation. Nat. Rev. Genet. *18*, 245–258. https://doi.org/10.1038/nrg.2016.167.

68. Kvon, E.Z., Kamneva, O.K., Melo, U.S., Barozzi, I., Osterwalder, M., Mannion, B.J., Tissières, V., Pickle, C.S., Plajzer-Frick, I., Lee, E.A., et al. (2016). Progressive Loss of Function in a Limb Enhancer during Snake Evolution. Cell *167*, 633–642.e11. https://doi.org/10.1016/j.cell.2016.09.028.

69. Wang, Z., Li, X., Yang, J., Gong, Y., Zhang, H., Qiu, X., Liu, Y., Zhou, C., Chen, Y., Greenbaum, J., et al. (2021). Single-cell RNA sequencing deconvolutes the in vivo heterogeneity of human bone marrow-derived mesenchymal stem cells. Int. J. Biol. Sci. *17*, 4192–4206. https://doi.org/10.7150/ijbs.61950.

70. Kun, E., Javan, E.M., Smith, O., Gulamali, F., de la Fuente, J., Flynn, B.I., Vajrala, K., Trutner, Z., Jayakumar, P., Tucker-Drob, E.M., et al. (2023). The genetic architecture and evolution of the human skeletal form. Science *381*, eadf8009. https://doi.org/10.1126/science.adf8009.

71. Milind, N., Smith, C.J., Zhu, H., Gjorgjieva, T., Spence, J.P., and Pritchard, J.K. (2025). Buffering and non-monotonic behavior of gene dosage response curves for human complex traits. Preprint at medRxiv. https://doi.org/10.1101/2024.11.11.24317065.

72. Sollis, E., Mosaku, A., Abid, A., Buniello, A., Cerezo, M., Gil, L., Groza, T., Güneş, O., Hall, P., Hayhurst, J., et al. (2023). The NHGRI-EBI GWAS Catalog: knowledgebase and deposition resource. Nucleic Acids Res. *51*, D977–D985. https://doi.org/10.1093/nar/gkac1010.

73. Buniello, A., Suveges, D., Cruz-Castillo, C., Llinares, M.B., Cornu, H., Lopez, I., Tsukanov, K., Roldán-Romero, J.M., Mehta, C., Fumis, L., et al. (2025). Open Targets Platform: facilitating therapeutic hypotheses building in drug discovery. Nucleic Acids Res. *53*, D1467–D1475. https://doi.org/10.1093/nar/gkae1128.

74. MacDonald, J.R., Ziman, R., Yuen, R.K.C., Feuk, L., and Scherer, S.W. (2014). The Database of Genomic Variants: a curated collection of structural variation in the human genome. Nucleic Acids Res. *42*, D986–D992. https://doi.org/10.1093/nar/gkt958.

75. Collins, R.L., Brand, H., Karczewski, K.J., Zhao, X., Alföldi, J., Francioli, L. C., Khera, A.V., Lowther, C., Gauthier, L.D., Wang, H., et al. (2020). A structural variation reference for medical and population genetics. Nature *581*, 444–451. https://doi.org/10.1038/s41586-020-2287-8.

76. Bu, C., Zheng, X., Zhao, X., Xu, T., Bai, X., Jia, Y., Chen, M., Hao, L., Xiao, J., Zhang, Z., et al. (2024). GenBase: A Nucleotide Sequence Database. Genomics Proteomics Bioinformatics *22*, qzae047. https://doi.org/10.1093/gpbjnl/qzae047.

77. CNCB-NGDC Members and Partners (2024). Database Resources of the National Genomics Data Center, China National Center for Bioinformation in 2024. Nucleic Acids Res. *52*, D18–D32. https://doi.org/10.1093/nar/gkad1078.

78. Okhovat, M., Nevonen, K.A., Davis, B.A., Michener, P., Ward, S., Milhaven, M., Harshman, L., Sohota, A., Fernandes, J.D., Salama, S.R., et al. (2020). Co-option of the lineage-specific LAVA retrotransposon in the gibbon genome. Proc. Natl. Acad. Sci. USA *117*, 19328–19338. https://doi.org/10.1073/pnas.2006038117.

79. Langmead, B., and Salzberg, S.L. (2012). Fast gapped-read alignment with Bowtie 2. Nat. Methods *9*, 357–359. https://doi.org/10.1038/nmeth.1923.

80. Servant, N., Varoquaux, N., Lajoie, B.R., Viara, E., Chen, C.-J., Vert, J.-P., Heard, E., Dekker, J., and Barillot, E. (2015). HiC-Pro: an optimized and flexible pipeline for Hi-C data processing. Genome Biol. *16*, 259. https://doi.org/10.1186/s13059-015-0831-x.

81. Xu, Z., and Wang, H. (2007). LTR_FINDER: an efficient tool for the prediction of full-length LTR retrotransposons. Nucleic Acids Res. *35*, W265–W268. https://doi.org/10.1093/nar/gkm286.

82. Gremme, G., Steinbiss, S., and Kurtz, S. (2013). GenomeTools: a comprehensive software library for efficient processing of structured genome annotations. IEEE/ACM Trans. Comput. Biol. Bioinform. *10*, 645–656. https://doi.org/10.1109/TCBB.2013.68.

83. Ou, S., and Jiang, N. (2018). LTR_retriever: a highly accurate and sensitive program for identification of long terminal repeat retrotransposons. Plant Physiol. *176*, 1410–1422. https://doi.org/10.1104/pp.17.01310.

84. Flynn, J.M., Hubley, R., Goubert, C., Rosen, J., Clark, A.G., Feschotte, C., and Smit, A.F. (2020). RepeatModeler2 for automated genomic discovery of transposable element families. Proc. Natl. Acad. Sci. USA *117*, 9451–9457. https://doi.org/10.1073/pnas.1921046117.

85. Chen, N. (2004). Using Repeat Masker to identify repetitive elements in genomic sequences. Curr. Protoc. Bioinformatics *Chapter 4*, Unit 4.10.

86. Talenti, A., and Prendergast, J. (2021). nf-LO: A Scalable, Containerized Workflow for Genome-to-Genome Lift Over. Genome Biol. Evol. *13*, evab183. https://doi.org/10.1093/gbe/evab183.

87. Harris, R.S. (2007). Improved Pairwise Alignment of Genomic DNA (Pennsylvania State University).

88. Armstrong, J., Hickey, G., Diekhans, M., Fiddes, I.T., Novak, A.M., Deran, A., Fang, Q., Xie, D., Feng, S., Stiller, J., et al. (2020). Progressive Cactus is a multiple-genome aligner for the thousand-genome era. Nature *587*, 246–251. https://doi.org/10.1038/s41586-020-2871-y.

89. Hickey, G., Paten, B., Earl, D., Zerbino, D., and Haussler, D. (2013). HAL: a hierarchical format for storing and analyzing multiple genome alignments. Bioinformatics *29*, 1341–1342. https://doi.org/10.1093/bioinformatics/btt128.

90. Hubisz, M.J., Pollard, K.S., and Siepel, A. (2011). PHAST and RPHAST: phylogenetic analysis with space/time models. Brief. Bioinform. *12*, 41–51. https://doi.org/10.1093/bib/bbq072.

91. Bolger, A.M., Lohse, M., and Usadel, B. (2014). Trimmomatic: a flexible trimmer for Illumina sequence data. Bioinformatics *30*, 2114–2120. https://doi.org/10.1093/bioinformatics/btu170.

92. Li, H. (2013). Aligning sequence reads, clone sequences and assembly contigs with BWA-MEM. Preprint at arXiv.

93. Danecek, P., Bonfield, J.K., Liddle, J., Marshall, J., Ohan, V., Pollard, M. O., Whitwham, A., Keane, T., McCarthy, S.A., Davies, R.M., et al. (2021). Twelve years of SAMtools and BCFtools. GigaScience *10*, giab008. https://doi.org/10.1093/gigascience/giab008.

94. Quinlan, A.R., and Hall, I.M. (2010). BEDTools: a flexible suite of utilities for comparing genomic features. Bioinformatics *26*, 841–842. https://doi.org/10.1093/bioinformatics/btq033.

95. McKenna, A., Hanna, M., Banks, E., Sivachenko, A., Cibulskis, K., Kernytsky, A., Garimella, K., Altshuler, D., Gabriel, S., Daly, M., et al. (2010). The Genome Analysis Toolkit: a MapReduce framework for analyzing next-generation DNA sequencing data. Genome Res. *20*, 1297–1303. https://doi.org/10.1101/gr.107524.110.

96. Li, H. (2018). Minimap2: pairwise alignment for nucleotide sequences. Bioinformatics *34*, 3094–3100. https://doi.org/10.1093/bioinformatics/bty191.

97. Heller, D., and Vingron, M. (2021). SVIM-asm: structural variant detection from haploid and diploid genome assemblies. Bioinformatics *36*, 5519–5521. https://doi.org/10.1093/bioinformatics/btaa1034.

98. Smolka, M., Paulin, L.F., Grochowski, C.M., Horner, D.W., Mahmoud, M., Behera, S., Kalef-Ezra, E., Gandhi, M., Hong, K., Pehlivan, D., et al. (2024). Detection of mosaic and population-level structural variants with Sniffles2. Nat. Biotechnol. *42*, 1571–1580. https://doi.org/10.1038/s41587-023-02024-y.

99. Kirsche, M., Prabhu, G., Sherman, R., Ni, B., Battle, A., Aganezov, S., and Schatz, M.C. (2023). Jasmine and Iris: population-scale structural variant comparison and analysis. Nat. Methods *20*, 408–417. https://doi.org/10.1038/s41592-022-01753-3.

100. McLaren, W., Gil, L., Hunt, S.E., Riat, H.S., Ritchie, G.R.S., Thormann, A., Flicek, P., and Cunningham, F. (2016). The Ensembl Variant Effect Predictor. Genome Biol. *17*, 122. https://doi.org/10.1186/s13059-016-0974-4.

101. Kim, D., Paggi, J.M., Park, C., Bennett, C., and Salzberg, S.L. (2019). Graph-based genome alignment and genotyping with HISAT2 and HISAT-genotype. Nat. Biotechnol. *37*, 907–915. https://doi.org/10.1038/s41587-019-0201-4.

102. Liao, Y., Smyth, G.K., and Shi, W. (2014). featureCounts: an efficient general purpose program for assigning sequence reads to genomic features. Bioinformatics *30*, 923–930. https://doi.org/10.1093/bioinformatics/btt656.

103. Kozlov, A.M., Darriba, D., Flouri, T., Morel, B., and Stamatakis, A. (2019). RAxML-NG: a fast, scalable and user-friendly tool for maximum likelihood phylogenetic inference. Bioinformatics *35*, 4453–4455. https://doi.org/10.1093/bioinformatics/btz305.

104. Mirarab, S., Reaz, R., Bayzid, M.S., Zimmermann, T., Swenson, M.S., and Warnow, T. (2014). ASTRAL: genome-scale coalescent-based species tree estimation. Bioinformatics *30*, i541–i548. https://doi.org/10.1093/bioinformatics/btu462.

105. Sayyari, E., Whitfield, J.B., and Mirarab, S. (2018). DiscoVista: Interpretable visualizations of gene tree discordance. Mol. Phylogenet. Evol. *122*, 110–115. https://doi.org/10.1016/j.ympev.2018.01.019.

106. Flouri, T., Jiao, X., Rannala, B., and Yang, Z. (2018). Species Tree Inference with BPP Using Genomic Sequences and the Multispecies Coalescent. Mol. Biol. Evol. *35*, 2585–2593. https://doi.org/10.1093/molbev/msy147.

107. Mailund, T., Dutheil, J.Y., Hobolth, A., Lunter, G., and Schierup, M.H. (2011). Estimating divergence time and ancestral effective population size of Bornean and Sumatran orangutan subspecies using a coalescent hidden Markov model. PLoS Genet. *7*, e1001319. https://doi.org/10.1371/journal.pgen.1001319.

108. Mailund, T., Halager, A.E., Westergaard, M., Dutheil, J.Y., Munch, K., Andersen, L.N., Lunter, G., Prüfer, K., Scally, A., Hobolth, A., et al. (2012). A New Isolation with Migration Model along Complete Genomes Infers Very Different Divergence Processes among Closely Related Great Ape Species. PLoS Genet. *8*, e1003125. https://doi.org/10.1371/journal.pgen.1003125.

109. Chang, C.C., Chow, C.C., Tellier, L.C., Vattikuti, S., Purcell, S.M., and Lee, J.J. (2015). Second-generation PLINK: rising to the challenge of larger and richer datasets. GigaScience *4*, 7. https://doi.org/10.1186/s13742-015-0047-8.

110. Pickrell, J.K., and Pritchard, J.K. (2012). Inference of population splits and mixtures from genome-wide allele frequency data. PLoS Genet. *8*, e1002967. https://doi.org/10.1371/journal.pgen.1002967.

111. Patterson, N., Moorjani, P., Luo, Y., Mallick, S., Rohland, N., Zhan, Y., Genschoreck, T., Webster, T., and Reich, D. (2012). Ancient admixture in human history. Genetics *192*, 1065–1093. https://doi.org/10.1534/genetics.112.145037.

112. Renaud, G., Stenzel, U., and Kelso, J. (2014). leeHom: adaptor trimming and merging for Illumina sequencing reads. Nucleic Acids Res. *42*, e141. https://doi.org/10.1093/nar/gku699.

113. Briggs, A.W., Good, J.M., Green, R.E., Krause, J., Maricic, T., Stenzel, U., Lalueza-Fox, C., Rudan, P., Brajković, D., Kućan, Z., et al. (2009). Targeted Retrieval and Analysis of Five Neandertal mtDNA Genomes. Science *325*, 318–321. https://doi.org/10.1126/science.1174462.

114. Ginolhac, A., Rasmussen, M., Gilbert, M.T.P., Willerslev, E., and Orlando, L. (2011). mapDamage: testing for damage patterns in ancient DNA sequences. Bioinformatics *27*, 2153–2155. https://doi.org/10.1093/bioinformatics/btr347.

115. Dierckxsens, N., Mardulyn, P., and Smits, G. (2017). NOVOPlasty: de novo assembly of organelle genomes from whole genome data. Nucleic Acids Res. *45*, e18. https://doi.org/10.1093/nar/gkw955.

116. Edgar, R.C. (2004). MUSCLE: multiple sequence alignment with high accuracy and high throughput. Nucleic Acids Res. *32*, 1792–1797. https://doi.org/10.1093/nar/gkh340.

117. Capella-Gutiérrez, S., Silla-Martínez, J.M., and Gabaldón, T. (2009). trimAl: a tool for automated alignment trimming in large-scale phylogenetic

analyses. Bioinformatics *25*, 1972–1973. https://doi.org/10.1093/bioinformatics/btp348.

118. Stamatakis, A. (2014). RAxML version 8: a tool for phylogenetic analysis and post-analysis of large phylogenies. Bioinformatics *30*, 1312–1313. https://doi.org/10.1093/bioinformatics/btu033.
119. Suchard, M.A., Lemey, P., Baele, G., Ayres, D.L., Drummond, A.J., and Rambaut, A. (2018). Bayesian phylogenetic and phylodynamic data integration using BEAST 1.10. Virus Evol. *4*, vey016. https://doi.org/10.1093/ve/vey016.
120. Posada, D. (2008). jModelTest: Phylogenetic Model Averaging. Mol. Biol. Evol. *25*, 1253–1256. https://doi.org/10.1093/molbev/msn083.
121. Rambaut, A., Drummond, A.J., Xie, D., Baele, G., and Suchard, M.A. (2018). Posterior Summarization in Bayesian Phylogenetics Using Tracer 1.7. Syst. Biol. *67*, 901–904. https://doi.org/10.1093/sysbio/syy032.
122. Helfrich, P., Rieb, E., Abrami, G., Lücking, A., and Mehler, A. (2018). TreeAnnotator: Versatile Visual Annotation of Hierarchical Text Relations. In Proceedings of the Eleventh International Conference on Language Resources and Evaluation (LREC 2018) (European Language Resources Association [ELRA]).
123. Paradis, E., and Schliep, K. (2019). ape 5.0: an environment for modern phylogenetics and evolutionary analyses in R. Bioinformatics *35*, 526–528. https://doi.org/10.1093/bioinformatics/bty633.
124. Zizka, A., Silvestro, D., Andermann, T., Azevedo, J., Duarte Ritter, C., Edler, D., Farooq, H., Herdean, A., Ariza, M., Scharn, R., et al. (2019). CoordinateCleaner: Standardized cleaning of occurrence records from biological collection databases. Methods Ecol. Evol. *10*, 744–751. https://doi.org/10.1111/2041-210X.13152.
125. Leonardi, M., Hallett, E.Y., Beyer, R., Krapp, M., and Manica, A. (2023). pastclim 1.2: an R package to easily access and use paleoclimatic reconstructions. Ecography *2023*, e06481. https://doi.org/10.1111/ecog.06481.
126. Kass, J.M., Muscarella, R., Galante, P.J., Bohl, C.L., Pinilla-Buitrago, G. E., Boria, R.A., Soley-Guardia, M., and Anderson, R.P. (2021). ENMeval 2.0: Redesigned for customizable and reproducible modeling of species' niches and distributions. Methods Ecol. Evol. *12*, 1602–1608. https://doi.org/10.1111/2041-210X.13628.
127. Love, M.I., Huber, W., and Anders, S. (2014). Moderated estimation of fold change and dispersion for RNA-seq data with DESeq2. Genome Biol. *15*, 550. https://doi.org/10.1186/s13059-014-0550-8.
128. Wu, T., Hu, E., Xu, S., Chen, M., Guo, P., Dai, Z., Feng, T., Zhou, L., Tang, W., Zhan, L., et al. (2021). clusterProfiler 4.0: A universal enrichment tool for interpreting omics data. Innovation (Camb) *2*, 100141. https://doi.org/10.1016/j.xinn.2021.100141.
129. Sangpakdee, W., Tanomtong, A., Fan, X., Pinthong, K., Weise, A., and Liehr, T. (2016). Application of multicolor banding combined with heterochromatic and locus-specific probes identify evolutionary conserved breakpoints in Hylobates pileatus. Mol. Cytogenet. *9*, 17. https://doi.org/10.1186/s13039-016-0228-x.
130. Capozzi, O., Carbone, L., Stanyon, R.R., Marra, A., Yang, F.T., Whelan, C.W., de Jong, P.J., Rocchi, M., and Archidiacono, N. (2012). A comprehensive molecular cytogenetic analysis of chromosome rearrangements in gibbons. Genome Res. *22*, 2520–2528. https://doi.org/10.1101/gr.138651.112.
131. Jurka, J., Kapitonov, V.V., Pavlicek, A., Klonowski, P., Kohany, O., and Walichiewicz, J. (2005). Repbase Update, a database of eukaryotic repetitive elements. Cytogenet. Genome Res. *110*, 462–467. https://doi.org/10.1159/000084979.
132. Ashburner, M., Ball, C.A., Blake, J.A., Botstein, D., Butler, H., Cherry, J. M., Davis, A.P., Dolinski, K., Dwight, S.S., Eppig, J.T., et al. (2000). Gene Ontology: tool for the unification of biology. The Gene Ontology Consortium. Nat. Genet. *25*, 25–29. https://doi.org/10.1038/75556.
133. Kanehisa, M., Goto, S., Sato, Y., Furumichi, M., and Tanabe, M. (2012). KEGG for integration and interpretation of large-scale molecular data sets. Nucleic Acids Res. *40*, D109–D114. https://doi.org/10.1093/nar/gkr988.
134. Koonin, E.V., Fedorova, N.D., Jackson, J.D., Jacobs, A.R., Krylov, D.M., Makarova, K.S., Mazumder, R., Mekhedov, S.L., Nikolskaya, A.N., Rao, B.S., et al. (2004). A comprehensive evolutionary classification of proteins encoded in complete eukaryotic genomes. Genome Biol. *5*, R7. https://doi.org/10.1186/gb-2004-5-2-r7.
135. Mistry, J., Chuguransky, S., Williams, L., Qureshi, M., Salazar, G.A., Sonnhammer, E.L.L., Tosatto, S.C.E., Paladin, L., Raj, S., Richardson, L.J., et al. (2021). Pfam: The protein families database in 2021. Nucleic Acids Res. *49*, D412–D419. https://doi.org/10.1093/nar/gkaa913.
136. Apweiler, R., Bairoch, A., Wu, C.H., Barker, W.C., Boeckmann, B., Ferro, S., Gasteiger, E., Huang, H., Lopez, R., Magrane, M., et al. (2004). UniProt: the Universal Protein knowledgebase. Nucleic Acids Res. *32*, D115–D119. https://doi.org/10.1093/nar/gkh131.
137. Paradis, E., Claude, J., and Strimmer, K. (2004). APE: Analyses of Phylogenetics and Evolution in R language. Bioinformatics *20*, 289–290. https://doi.org/10.1093/bioinformatics/btg412.
138. Akaike, H. (1974). A new look at the statistical model identification. IEEE Trans. Autom. Control *19*, 716–723. https://doi.org/10.1109/TAC.1974.1100705.
139. Britton, T., Oxelman, B., Vinnersten, A., and Bremer, K. (2002). Phylogenetic dating with confidence intervals using mean path lengths. Mol. Phylogenet. Evol. *24*, 58–65. https://doi.org/10.1016/S1055-7903(02)00268-3.
140. Dabney, J., Knapp, M., Glocke, I., Gansauge, M.-T., Weihmann, A., Nickel, B., Valdiosera, C., García, N., Pääbo, S., Arsuaga, J.-L., et al. (2013). Complete mitochondrial genome sequence of a Middle Pleistocene cave bear reconstructed from ultrashort DNA fragments. Proc. Natl. Acad. Sci. USA *110*, 15758–15763. https://doi.org/10.1073/pnas.1314445110.
141. Kircher, M., Sawyer, S., and Meyer, M. (2012). Double indexing overcomes inaccuracies in multiplex sequencing on the Illumina platform. Nucleic Acids Res. *40*, e3. https://doi.org/10.1093/nar/gkr771.
142. Fu, Q., Meyer, M., Gao, X., Stenzel, U., Burbano, H.A., Kelso, J., and Pääbo, S. (2013). DNA analysis of an early modern human from Tianyuan Cave, China. Proc. Natl. Acad. Sci. USA *110*, 2223–2227. https://doi.org/10.1073/pnas.1221359110.
143. Finstermeier, K., Zinner, D., Brameier, M., Meyer, M., Kreuz, E., Hofreiter, M., and Roos, C. (2013). A Mitogenomic Phylogeny of Living Primates. PLoS One *8*, e69504. https://doi.org/10.1371/journal.pone.0069504.
144. Scally, A., and Durbin, R. (2012). Revising the human mutation rate: implications for understanding human evolution. Nat. Rev. Genet. *13*, 745–753. https://doi.org/10.1038/nrg3295.
145. Germain, R.R., Feng, S., Chen, G., Graves, G.R., Tobias, J.A., Rahbek, C., Lei, F., Fjeldså, J., Hosner, P.A., Gilbert, M.T.P., et al. (2023). Species-specific traits mediate avian demographic responses under past climate change. Nat. Ecol. Evol. *7*, 862–872. https://doi.org/10.1038/s41559-023-02055-3.
146. Krapp, M., Beyer, R.M., Edmundson, S.L., Valdes, P.J., and Manica, A. (2021). A statistics-based reconstruction of high-resolution global terrestrial climate for the last 800,000 years. Sci. Data *8*, 228. https://doi.org/10.1038/s41597-021-01009-3.
147. Yaworsky, P.M., Nielsen, E.S., and Nielsen, T.K. (2024). The Neanderthal niche space of Western Eurasia 145 ka to 30 ka ago. Sci. Rep. *14*, 7788. https://doi.org/10.1038/s41598-024-57490-4.
148. Lobo, J.M., Jiménez-Valverde, A., and Real, R. (2008). AUC: a misleading measure of the performance of predictive distribution models. Glob. Ecol. Biogeogr. *17*, 145–151. https://doi.org/10.1111/j.1466-8238.2007.00358.x.

STAR★METHODS

KEY RESOURCES TABLE

REAGENT or RESOURCE	SOURCE	IDENTIFIER
Critical commercial assays		
TRIzol reagent	Thermo scientific	N/A
RNeasy mini kit	Qiagen	N/A
PrimerScript RT Reagent kit	Vazyme Biotech	N/A
ARS staining kit for osteogenesis	Beyotime	N/A
Deposited data		
Pileated gibbon (*Hylobates pileatus*) genome assembly	This paper; Shao et al.[24]	Genome Warehouse in National Genomic Data Center (https://ngdc.cncb.ac.cn/gwh): GWHFIUL00000000.1
Southern white-cheeked gibbon (*Nomascus siki*) genome assembly	This paper; Shao et al.[24]	Genome Warehouse in National Genomic Data Center (https://ngdc.cncb.ac.cn/gwh): GWHFIUK00000000.1
Eastern hoolock gibbon (*Hoolock leuconedys*) genome assembly	This paper; Shao et al.[24]	Genome Warehouse in National Genomic Data Center (https://ngdc.cncb.ac.cn/gwh): GWHFIUM00000000.1
Siamang (*Hoolock leuconedys*) genome assembly	This paper; Shao et al.[24]	Genome Warehouse in National Genomic Data Center (https://ngdc.cncb.ac.cn/gwh): GWHFIUJ00000000.1
Raw Short-read sequencing data	This paper; Carbone et al.[8]; Kuderna et al.[60]; Okhovat et al.[78]	National Genomic Data Center: PRJCA035014; NCBI: PRJNA232723, PRJNA564127; EBI: PRJEB59576
Raw Hi-C data	This paper	National Genomic Data Center: PRJCA035014
Raw RNA sequencing data	This paper	National Genomic Data Center: PRJCA042400
Experimental models: Cell lines		
Human: Human bone marrow mesenchymal stem cell lines (hBMSCs)	hBMSC, Oricell, HUXMF-01001, China	N/A
Human: human embryonic kidney cells (239T)	239T, Kunming Institue of Zoology, CAS, China	N/A
Experimental models: Organisms/strains		
Mouse: human-SHH-3'UTR-gibbon-deletion knock-in (Mus musculus, C57BL/6J)	Shanghai Model Organisms Center, Inc. (Shanghai, China)	N/A
Oligonucleotides		
qRT-PCR primers for GAPDH: Forward: GACAGTCAGCCGCATCTTCT, Reverse: GCCCAATACGACCAAATCCGT	This paper	N/A
qRT-PCR primers for SHH: Forward: TCTCCAGAAACTCCGAGCGA, Reverse: CTCCCCGGGGTTTTTGCTT	This paper	N/A
qRT-PCR primers for GLI1: Forward: CGCCCAGACAGAGTGTCC, Reverse: GTCCTTCTGTCCCCACACTG	This paper	N/A

(*Continued on next page*)

Continued

REAGENT or RESOURCE	SOURCE	IDENTIFIER
CRISPR/Cas9 gRNA: sequence 1: AGCTGAAGCCCGACGGGACC GGG, sequence 2: GAAAATATCTACTGACC ACT GGG	This paper	N/A
Software and algorithms		
Bowtie2	Langmead and Salzberg[79]	https://github.com/BenLangmead/bowtie2
HiC-Pro v2.8.0	Servant et al.[80]	https://github.com/nservant/HiC-Pro/
LACHESIS	Burton et al.[27]	https://github.com/shendurelab/LACHESIS
RagTag	Alonge et al.[28]	https://github.com/malonge/RagTag
LTR_Finder	Xu and Wang[81]	https://github.com/xzhub/LTR_Finder
GenomeTools v1.6.1	Gremme et al.[82]	https://github.com/shendurelab/LACHESIS
LTR_retriever v2.9.0	Ou and Jiang[83]	https://github.com/oushujun/LTR_retriever
RepeatModeler v2.0.1	Flynn et al.[84]	http://www.repeatmasker.org/
RepeatMasker v1.33.1	Chen[85]	http://www.repeatmasker.org/
AUGUSTUS v3.3.2	Stanke[30]	https://github.com/Gaius-Augustus/Augustus
GeneWise v2.4.1	Birney et al.[29]	https://www.ebi.ac.uk/~birney/wise2
nf-LO v1.8.0	Talenti and Prendergast[86]	https://github.com/evotools/nf-LO
LASTZ	Harris[87]	https://github.com/lastz/lastz
Cactus v2.6.0	Armstrong et al.[88]	https://github.com/ComparativeGenomicsToolkit/cactus
Haltools v2.3	Hickey et al.[89]	https://github.com/ComparativeGenomicsToolkit/hal
mafTools	Github	https://github.com/dentearl/mafTools
Phast	Hubisz et al.[90]	http://compgen.cshl.edu/phast/
Trimmomatic v0.39	Bolger et al.[91]	http://www.usadellab.org/cms/index.php?page=trimmomatic
BWA v0.7.17-r1188	Li[92]	https://github.com/lh3/bwa
SAMtools v1.16.1	Danecek et al.[93]	https://github.com/samtools/samtools
BCFtools v1.16.1	Danecek et al.[93]	https://github.com/samtools/bcftools
BEDTools v2.31.1	Quinlan and Hall[94]	https://github.com/arq5x/bedtools2
Genome Analysis Toolkit (GATK) v3.8-1	McKenna et al.[95]	https://gatk.broadinstitute.org/
Minimap2	Li[96]	https://github.com/lh3/minimap2
SVIM-asm	Heller and Vingron[97]	https://github.com/eldariont/svim-asm
Sniffles v2.2	Smolka et al.[98]	https://github.com/fritzsedlazeck/Sniffles
Jasmine v1.1.5	Kirsche et al.[99]	https://github.com/mkirsche/Jasmine
VEP v110	McLaren et al.[100]	https://github.com/Ensembl/ensembl-vep
Hisat2 v2.2.1	Kim et al.[101]	https://github.com/DaehwanKimLab/hisat2
Featurecounts v2.0.1	Liao et al.[102]	https://github.com/ShiLab-Bioinformatics/subread
RAxML-NG	Kozlov et al.[103]	https://github.com/amkozlov/raxml-ng
ASTRAL v5.1.1	Mirarab et al.[104]	https://github.com/smirarab/ASTRAL
DiscoVista v1.0	Sayyari et al.[105]	https://github.com/esayyari/DiscoVista
BPP v4.7.0	Flouri et al.[106]	https://github.com/bpp/bpp
CoalHMM with CI model	Mailund et al.[107]	https://github.com/mailund/IMCoalHMM
CoalHMM with IM model	Mailund et al.[108]	https://github.com/mailund/IMCoalHMM
CoalHMM with ILS model	Dutheil et al.[43]	https://github.com/jydu/coalhmm
PLINK v2.0	Chang et al.[109]	https://www.cog-genomics.org/plink/2.0/

(*Continued on next page*)

Continued		
REAGENT or RESOURCE	SOURCE	IDENTIFIER
TreeMix v1.13	Pickrell and Pritchard[110]	https://bitbucket.org/nygcresearch/treemix/wiki/Home
Admixtools v7.0.2	Patterson et al.[111]	https://github.com/DReichLab/AdmixTools
Dsuite	Malinsky et al.[52]	https://github.com/millanek/Dsuite
leeHom v1.2.17	Renaud et al.[112]	https://github.com/grenaud/leeHom
Mia v1.0	Briggs et al.[113]	https://github.com/mpieva/mapping-iterative-assembler
MapDamage v2.2.1	Ginolhac et al.[114]	https://github.com/ginolhac/mapDamage
Novoplasty v4.3.1	Dierckxsens et al.[115]	https://github.com/ndierckx/NOVOPlasty
Muscle v3.8.31	Edgar[116]	https://drive5.com/muscle/
trimAl v1.2	Capella-Gutiérrez et al.[117]	https://github.com/inab/trimal
RAxML v8.2.3	Stamatakis[118]	https://github.com/stamatak/standard-RAxML
BEAST v1.10.4	Suchard et al.[119]	https://beast.community/
jModelTest v2.1.10	Posada[120]	https://github.com/ddarriba/jmodeltest2
Tracer v1.7.2	Rambaut et al.[121]	https://github.com/beast-dev/tracer
TreeAnnotator v1.10.4	Helfrich et al.[122]	https://www.beast2.org/treeannotator/
FigTree v1.4.4	N/A	https://github.com/rambaut/figtree
PSMC v0.6.5	Li and Durbin[58]	https://github.com/lh3/psmc
R v4.4.0	N/A	https://www.R-project.org/
R package APE	Paradis and Schliep[123]	https://github.com/emmanuelparadis/ape
R package CoordinateCleaner	Zizka et al.[124]	https://cran.r-project.org/web/packages/CoordinateCleaner/index.html
R package pastclim v1.2	Leonardi et al.[125]	https://github.com/EvolEcolGroup/pastclim
R package raster	N/A	https://github.com/rspatial/raster
R package ENMeval v2.0	Kass et al.[126]	https://github.com/jamiemkass/ENMeval
R package tidyverse	N/A	https://tidyverse.tidyverse.org/
R package Deseq2	Love et al.[127]	https://github.com/thelovelab/DESeq2
R package clusterProfiler	Wu et al.[128]	https://github.com/YuLab-SMU/clusterProfiler
R package effsize	N/A	https://github.com/mtorchiano/effsize
R package ggridges	N/A	https://github.com/wilkelab/ggridges
SeProcessPro Analyser v1.0	Suzhou Heisfeld Information Technology Co. Ltd., China	N/A
Other		
Quantstudio 5 real-time PCR system	Thermo Scientific	N/A
High-resolution micro-CT instrument	Hiscan XM	N/A

EXPERIMENTAL MODEL AND STUDY PARTICIPANT DETAILS

Generating stable transfection cells

Lenti-vector *SHH*-gibbon-3'UTR-EGFP and *SHH*-human-3'UTR-EGFP (GV367) and packaged lentivirus were constructed by GeneChem (Shanghai, China). For lentiviral transfections, packaged lentivirus was transfected into hBMSCs as described in the instructions, and stably transfected cells were filtrated using puromycin at a concentration of 2μg/mL. The target cells were identified by observing EGFP using fluorescence microscopy and detecting *SHH* and *GLI1* expression using quantitative reverse transcription-PCR (qRT-PCR).

Human bone marrow mesenchymal stem cell lines (hBMSC, Oricell, HUXMF-01001, China) were cultured in a basal medium (Oricell, HUXMF-90011, China) containing 10% fetal bovine serum with culture supplement. All cells were incubated at 37°C with 5% CO_2. For osteogenic differentiation of cells, the cells were induced using an osteoblast differentiation medium (Oricell, China) as described in the instructions.

Generating CRISPR/Cas9 mice

The human-SHH-3'UTR-gibbon-deletion knock-in mice (*Mus musculus*, C57BL/6J) were designed by Shanghai Model Organisms Center, Inc. (Shanghai, China). Briefly, Cas9 mRNA and gRNA (gRNA sequence 1: AGCTGAAGCCCGACGGGACC GGG, gRNA sequence 2: GAAAATATCTACTGACCACT GGG) were generated, and a homologous recombination vector (donor vector) was constructed by in-fusion cloning that contained a 5' homology arm, the human-SHH-3'UTR-gibbon-deletion sequence, and a 3' homology arm. The donor vector, Cas9 mRNA, and gRNA were micro-injected into the fertilized eggs of C57BL/6J mice to generate the F0 generation mice. PCR amplification and sequencing were used to identify the positive F0 generation mice, which were then mated with wild C57BL/6J mice to obtain the positive F1 generation mice. All mice were bred and maintained in a barrier environment and kept in alternating light/darkness for 12 hours. This animal experiment was approved by the Institutional Animal Care and Use Committee at the Kunming Institute of Zoology, Chinese Academy of Science (Permit Number: IACUC-PE-2023-04-005), for animal welfare and ethics.

METHOD DETAILS

Genome scaffolding and annotation

Genome scaffolding

We applied Hi-C technology to assemble the genomes of *Ho. leuconedys* and *S. syndactylus* to chromosome-level (Table S1). Hi-C libraries were generated from two blood samples using a standard protocol. Briefly, after the completion crosslinking and lysis, chromatin was digested with 400 U of MboI restriction enzyme (NEB) at 37°C. The resulting DNA ends were labeled with biotin and incubated at 37°C for 45 min, followed by proximity ligation with T4 DNA ligase (NEB) for 4-6 hours. After ligation, proteinase K was added to reverse cross-linking during incubation at 65 °C overnight. DNA fragments were purified and dissolved in water. Unligated ends were then removed. The purified DNA was fragmented to a size of 350-500 bp. DNA fragments labeled by biotin were separated on Dynabeads® M-280 Streptavidin (Life Technologies). Final libraries were quality-controlled and sequenced on the MGI DNBSEQ-T7 platform. We used bowtie2[79] to align Hi-C reads to scaffolds, and the valid paired-end reads and contact maps were obtained following Hi-Pro pipelines.[80] Pseudo-chromosomes were produced by clustering, ordering and orienting the scaffolds using LACHESIS.[27] A heatmap was constructed using a bin size of 500kb, to test for accuracy based on the interaction signals. Based on the synteny with NLE (GenBank ID: GCF_006542625.1), we performed the genome scaffolding method RagTag[28] to the NSI genome. We made use of the synteny with human and the previously reported fluorescent in situ hybridization (FISH)[12,129,130] to assign the order and orientation of chromosomes.

Genome annotation

We identified repeat sequences using a combination of homology-based strategies and ab initio-based methods. We used LTR_Finder,[81] GenomeTools (v1.6.1),[82] LTR_retriever (v2.9.0)[83] and RepeatModeler (v2.0.1)[84] to build a *de novo* repeat library, and merged with RepBase dataset,[131] then RepeatMasker[85] was used to predict the repeats. For *de novo* gene structure prediction (Table S2), AUGUSTUS (3.3.2)[30] was used for *de novo* prediction. Protein-coding sequences of mouse (*Mus musculus*, GRCm38), human (*Homo sapiens*, GRCh38), chimpanzee (*Pan troglodytes*, GCF_002880755.1), gorilla (*Gorilla gorilla*, GCA_900006655.3) and orangutan (*Pongo abelii*, GCA_002880775.3) were used to homolog-based annotation using GeneWise (v2.4.1),[29] the final gene functional annotation were mapped to the following public databases: GO[132], KEGG[133], KOG,[134] NR, PFAM[135] and TrEMBL.[136]

Chromosome rearrangements in the gibbon genome

Based on chromosome-level genomes of the four genera, we compared chromosome rearrangements between the human and gibbon genome and among gibbon genomes. The pairwise genome alignment was conducted by a Nextflow pipeline nf-LO (v1.8.0)[86] with LASTZ[87] as aligner and the parameters "–distance primate –tgtSize 30000000 –tgtOvlp 100000 –srcSize 10000000".

Genome re-sequencing dataset collection and processing

Gibbon sample collection and genome re-sequencing

We collected a total of 75 individuals with short-read sequencing data, which encompassed 18 extant species, including 31 newly sequenced samples. The new samples were obtained from fresh blood, frozen tissue or fur from historical museum specimens, and sequenced on the Illumina sequencing platform. Samples were collected under the supervision of the Institutional Animal Care and Use Committee at the Kunming Institute of Zoology. Refer to Table S3 for detailed sample information.

Short read mapping and SNP calling

All newly generated and downloaded short reads of gibbons were filtered by Trimmomatic (v0.39),[91] and then aligned to their own genus reference genome (*Hylobates pileatus*, *Nomascus siki*, *Hoolock leuconedys* or *Symphalangus syndactylus*) using BWA-MEM (v0.7.12).[92] We applied SAMtools[93] to sort reads by genome coordinate and to remove duplicate reads in aligned BAM files. Because of superfluous alignment errors around indels, we performed a two-step indel realignment using RealignerTargetCreator and IndelRealigner in the Genome Analysis Toolkit (GATK) (v3.8-1).[95] Then, GATK subcommands: HaplotypeCaller, CombineGVCFs and GenotypeGVCFs were used to generate GVCFs, combine GVCFs, and genotype SNPs and indels from GVCFs.

Generating genome consensus sequence

The genome consensus sequences of high-depth sequencing individuals were generated from BAM files using samtools-bcftools pipeline. We filtered out the genomic regions with a depth below 1/3 x mean depth or above 10 x mean depth in each sample

and ignored short indel variants. The heterozygous sites were replaced with degenerated bases. The final genomic coordinates of the consensus sequences are the same as in the reference.

Phylogeny and incomplete lineage sorting across four gibbon genera

Multiple-genome alignment

The multiple genome alignment was conducted by Cactus (v2.6.0).[88] We used the star tree: "((HLE, HPI, NSI, SSY), Human);" as the input species tree without presetting phylogenetic hypotheses. The hal2maf command in haltools[89] was applied for converting HAL alignment to MAF alignment with parameters "–keepEmptyRefBlocks –onlyOrthologs –unique –noAncestors –refGenome Human". We removed the duplicates originating from the same species in the alignment blocks using mafDuplicateFilter from mafTools (https://github.com/dentearl/mafTools).

Gene CDS tree and 4-fold degenerate sites tree

We used the msa_view from phast package[90] to extract 4-fold degenerate sites and CDS from multiple genome alignment based on human gene annotation (Ensembl V110). A maximum-likelihood (ML) phylogenetic tree was inferred with RAxML-NG (*29*) with the GTR+ Γ model, 100 rapid bootstrap replications and human as outgroup. As for the CDS phylogenetic tree, we removed the CDSs lacking length of multiples of three, and partitioned the CDSs with the first two codon positions and third codon position.

Sliding window tree

Based on the multiple genome alignment from Cactus, we split the genome into different non-overlapping windows of size 50kb, 100kb, 500kb and 1Mbp, respectively. We discarded the windows containing >50% missing bases in total. ML phylogenetic inference was carried out with RAxML-NG[103] with the $GTR+\Gamma$ model, 100 rapid bootstrap replications and human as outgroup. Short internal branches originating from rapid speciation in a phylogenic tree often suffer from an empirical anomaly zone,[39] and result in a gene tree with high proportion that is inconsistent with the species tree. The phylogeny derived from the three species is free of the anomaly zone. For testing the anomaly zone in the phylogeny of gibbons, we inferred the ML tree using four species (HLE-SSY-NSI-HPI) and three species (HLE-NSI-HPI, SSY-NSI-HPI, HPI-HLE-SSY, NSI-HLE-SSY), respectively. The Tree topology, rate of node support and branch-length statistics were performed with the APE package[137] in R language. Next, we built the coalescent species tree from sliding-window trees using ASTRAL,[104] and the tree discordance was visualized with DiscoVista.[105]

Coalescent-based tree

We generated a non-coding dataset from multiple genome alignments from Cactus by removing CPG-islands, genic and repeat regions, and extracting loci that are at least 50kbp apart from each other, consisting of a total length of 112 Mbp and 71,960 loci with lengths ranging from 1kbp to 12kbp. We applied the A01 analysis in Bayesian program BPP (v4.7.0)[106] to infer the coalescent-based species tree under the multi-species coalescent model (MSC). We used $\theta \sim IG(3, 0.003)$ and $\tau_0 \sim IG(3, 0.04)$ for the priors of the parameters. Owing to the intensive computation and potential MCMC mixing issues in large datasets, we split the noncoding loci into 144 smaller subsets, each consisting of 500 loci. For each dataset, we performed 12 independent runs with varying starting species trees. The MCMC samples were taken every 5 iterations with a total of 2.5×10^6 samples, after a burn-in of 1×10^5. Finally, we summarized the probabilities of all posterior trees and designated the one with the highest probability as the species tree.

CoalHMM with ILS model

We applied the CoalHMM with ILS model[43] to the 1Mbp non-overlapping windows of the multiple genome alignment above. According to the species tree of the four gibbon genera (*Hylobates*, (*Nomascus*, (*Hoolock*, *Symphalangus*))), we used four three-species combinations: (HPI,(NSI,HLE)), (HPI,(NSI,SSY)), (HPI,(HLE,SSY)), and (NSI,(HLE,SSY)). In the standard coalescent model, the probability of incongruent trees depends on both the time interval between two speciation events (ΔT, in generations), the ancestral effective population size (N_{eA})[35]:

$$\Pr\left(\textit{incongruent trees}\right) = \frac{2}{3}e^{(-\Delta T/(2N_{eA}))}$$

and the probability of species trees equals to $1 - \frac{2}{3}e^{(-\Delta T/(2N_{eA}))}$.

CoalHMM with complete isolation (CI-CoalHMM) and isolation with migration (IM-CoalHMM) model

A coalescent hidden Markov model, CoalHMM, was used to estimate the ancestral effective population size and divergence times of pairs of gibbons within genera with complete isolation (CI-CoalHMM)[107] and isolation with migration (IM-CoalHMM; can detect gene flow during the process of speciation)[108] models. For pairs of gibbons, we used the consensus sequence of high-coverage short read re-sequencing samples. We filtered out the windows with more than 50% missing sequence or where (1) the recombination rate was below 0.01cM/Mbp or above 10cM/Mbp, (2) the ancestral effective population size below 1,000 or above 1,000,000 or (3) the split time was below 5,000 or above 10 million years for gibbon species pairs. The median pairwise divergence times were mapped to the species tree. Akaike information criteria (AIC)[138] were used for model selection as described by Mailund et al.[108] We applied the mean path length (MPL) method (chronoMPL)[139] in the APE package[123] to generate ultrametirc tree.

Phylogeny and gene flow among three gibbon genera

Phylogeny based on whole-genome SNPs

The identity-by-state (IBS) distance matrix was calculated from whole-genome SNPs using PLINK2.[109] The neighbor-joining (NJ) tree (Figure S4) was then estimated by the APE package[123] in R. The genome-wide allele frequency of SNPs were used to construct the

ML tree with TreeMix.[110] Considering the linkage disequilibrium of nearby SNPs and the single individuals in some species, we added the parameters "-k 1000" (1000 SNPs per block for estimation of covariance matrix) and "-noss" (turn off sample size correction) to the running commands. We ran TreeMix 100 times to perform bootstrapping by adding the parameter "-bootstrap".

Inference of gene flow within the three genera

D-statistics implemented in Admixtools[111] was applied to analyze gene flow among different species within three gibbon genera. The standard error and Z-score of the D-statistic were then computed based on the variation of the weighted jackknife replicates using 5Mb non-overlapping genomic blocks. The f-branch statistic[53] in D-suite[52] was performed to place the introgression events on the phylogeny within species in the three gibbon genera. Because of different reference genomes across the three gibbon genera, we independently used D-suite to estimate gene flow within genera, and plotted the results into one figure (Figure 4B).

Phylogenetic analysis using ancient and extant gibbon mitochondrial DNA

Ancient DNA extraction, sequencing, and filtering

Ancient DNA (aDNA) extraction and library construction were carried out in the ancient DNA laboratory at the Institute of Vertebrate Paleontology and Paleoanthropology, Chinese Academy of Sciences. 251, 99 and 126 mg of bone or teeth powder were collected from Junzi (JZ_2k) at Shenheyuan tomb, Longlindong Cave (CZ_50k) at Chongzuo and Yemao Cave (YMD_4k) at Chongqing, respectively. DNA extraction of the three ancient gibbon specimens followed an aDNA extraction protocol described previously.[140] In total, 30 single-strand (SS) libraries were constructed (11 libraries for sample CZ_50k, 13 libraries for sample YMD_4k, and 6 libraries for sample JZ_2k) with uracil-DNA-glycosylase (UDG) treatment to retain the ancient DNA damage characteristics; for detailed information, see Tables S6 and S7. DNA amplification was performed on AccuPrime Pfx DNA polymerase with 35 cycles to ensure sufficient DNA for the capture process. During this amplification process, sample-specific barcodes were attached to each P5 and P7 library adaptors to avoid downstream cross-contamination of libraries.[141] Then, PCR products were purified with the MinElute PCR purification kit (Qiagen, Hilden, Germany), and the library concentrations were measured with a NanoDrop 2000 spectrophotometer. The oligonucleotide probes were used to capture the mitochondrial genome as described in a previous study.[142] High-throughput sequencing was then performed for the enriched library pools on the Illumina Miseq platform with $2 \times 76 + 2 \times 7$ cycles. The overlapping sequences were merged with the parameter "–ancientdna", and the adapter sequences were trimmed using the program leeHom.[112] After merging, all fragments were aligned to the *N. leucogenys* mtDNA reference (GenBank: NC_021957).[143] MIA (v1.0)[113] was used for assembling the consensus sequences with parameters "-C -c -H 1 -k 12". For considering the authenticity of the ancient DNA sequence, the post-mortem damage patterns for each sample were assessed using MapDamage (v2.2.1).[114] Then, we masked the 5bp at the end of the fragments (C -> T) to minimize the influence of cytosine deamination.

Mitochondrial genome assembly

The *de novo* genome assembly tool Novoplasty[115] was used to construct the whole mitochondrial genomes from paired-end short reads. The complete mitochondrial sequence of the northern white-cheeked gibbon (*N. leucogenys*, GeneBank accession number: NC_021957)[143] was used as a seed and reference input. Only complete circularized mitochondrial sequences (Table S5) were used for downstream analysis. For the mitogenome of Hainan gibbon, we performed the short-read mapping method to call the consensus sequence from BAM file using samtools. The whole mitogenome of an eastern black crested gibbon (*Nomascus nasutus*) was generated from DNA extracted from a fecal sample which has been collected in Trung Khanh Nature Reserve, Cao Bang Province, Vietnam in 2008. DNA was extracted with the Qiagen Stool Mini Kit. The whole mitogenome was generated via 20 overlapping PCR products with a length of 1.0-1.2 kb followed by Sanger sequencing.

Mitochondrial genome tree and divergence time

Multiple sequences were aligned with MUSCLE (v3.8.31)[116] and filtered using trimAl (v1.2rev59)[117] with parameters "-gt 0.8 -cons 60 -w 3". The phylogenetic trees with 78 or 112 ancient and present-day gibbon mitogenomes were constructed using the ML method implemented in RAxML (v8.2.3)[118] with multiple nucleotide substitution models. The preliminary tree for the optimization was constructed using the GTRCAT model in RAxML. Phylogenetic inference was then implemented based on the first two codon positions and the third codon position of the complete mitogenomes using the GTRGMMA model in RAxML. The final trees after 1000 bootstrap replicates were generated using the GTRCAT model in RAxML and projected to the preliminary tree labeled with bootstrap values by taking the human (accession number: NC_012920) reference mitogenome as the outgroup.

To further confirm the phylogeny and estimate divergence times, Bayesian framework-based phylogeny analysis was performed in BEAST (v1.10.4),[119] incorporating 78 complete gibbon mitogenomic sequences with high depth of the coverage. Five fossil records from the literatures (A, B, C, E, G described in Rivas-González et al.)[17] were used to calibrate the node age. The best-fit substitution model was determined under the Bayesian Information Criterion (BIC) using jmodeltest v2.1.10.[120] The best-site model was determined as GTR+G+I. To test whether a strict or a relaxed molecular clock was more suitable for the BEAST analysis, we checked the posterior density for the lognormal standard deviation, and the result showed the strict clock cannot be rejected (the density parameter ucld.stdev including 0). In addition, we also checked the coefficient of variation ($\sim$0) in Tracer[121] and obtained better support for the strict clock. Thus, we assumed a strict clock for the phylogenetic analysis. Prior distribution of the clock rate was set as a uniform distribution with an approximate range from $2e^{-9}$ to $2e^{-7}$, which fitted the characteristics of the majority of fast or moderate evolving mammals in their mitogenomes including primates.[144]

For the choice of tree prior, three models (constant size, Skyline piecewise-constant, and Skyline piecewise-linear) were tested. We used log marginal likelihoods estimated by Path-Sampling (PS) and Stepping-Stone (SS) methods to determine the best model.

The best model was the Skyline piecewise-linear (PS and SS values: -130573.4 and -130569.3) followed by constant size (-130611.8 and -130609.8) and Skyline piecewise-constant (-131050.2 and -130952.9). We ran 40 million MCMC chains, sampling every 1000 steps, to ensure the effective sample size (ESS) values were greater than 300. All chains converged in Tracer, and a total of 10% of the trees were discarded as burn-in using TreeAnnotator (v1.10.4)[122] and we visualized the phylogeny in FigTree (v1.4.4). We estimated a mutation rate of 1.78×10^{-8} (95% HPD, 1.55×10^{-8}–2.02×10^{-8}) substitutions/site/year across the complete mtDNA genomes for the gibbon family.

Population history and genetic diversity analysis

Pairwise sequentially Markovian coalescent (PSMC) analysis

To reconstruct the fluctuation in effective population sizes of gibbons over the past 5 million years, we applied the Pairwise Sequentially Markovian Coalescent (PSMC)[58] model, based on high-depth sequenced individuals (Table S3). For facilitating comparisons, we analyzed each of the genomes using the same parameter ("-N 25 -t 15 -r 5 -p 1*4+25*2+4+6") as described by Carbone et al.[8] 100 bootstrap replications were performed by randomly sampling with replacement the 500Kbp segments of gibbon genomes. We assumed the same neutral mutation rate $\mu = 1 \times 10^{-8}$ per site per generation[8] and a generation time $g = 15$ years[44] for all gibbon species. To reveal shared dynamic trends of effective population size (N_e) across all gibbon species, while accounting for differences in absolute scales, we employed a normalization method used in several previous studies.[24,145] For each species, the normalized N_e at each time point was calculated by dividing the observed value by the maximum N_e value across the entire timescale. Subsequently, to visualize the overall population trajectory, we calculated the mean and s.d. of normalized N_e values for each genus at 120 equally spaced (log linear) time points.

Assessing the impact of introgression on PSMC inference

Because introgression can lead to overestimation of effective population size in PSMC analyses, we explicitly tested its impact on our demographic reconstructions. We used the sliding-window f_d statistic to identify genomic regions likely affected by introgression within the *Nomascus* and *Hylobates* genera, where we had previously detected gene flow. Specifically, we calculated f_d in 500 kb sliding windows with a 250 kb step size for the following comparisons, using an outgroup from a different genus: (1) For gene flow between HLA and HPI: f_d(HKL/HAG, HLA, HPI, Outgroup); (2) For gene flow between HMO and other Hylobates species: f_d(HAG, HMU/HFU/HAB, HMO, Outgroup) and f_d (HKL, HMO, HMU/HFU/HAB, Outgroup); (3) For gene flow between NCO and other Nomascus species: f_d (NGA/NAN, NSI/NLE, NCO, Outgroup). For each comparison, we calculated Z-scores for the f_d values, and windows with a Z-score > 2 were considered as putative introgressed regions. The introgressed regions identified from all relevant comparisons within each group were then merged to create final regions to be removed. This resulted in the masking of 214 Mb, 153 Mb, and 613 Mb of sequence for the NCO-NLE-NSI, HPI-HLA, and HMO-HMU-HFU-HAB introgression scenarios, respectively. We then performed PSMC analysis on these introgression-masked genomes using the same parameters as the primary analysis. The resulting demographic trajectories were compared to those from the original, unmasked analyses to assess the impact of introgression (supplemental information).

Heterozygosity and runs of homozygosity (ROH)

To estimate genome-wide and window-based heterozygosity, we applied the computational pipeline used in Kuderna et al.[60] In short, we generated the callable regions by removing genome positions that had below 1/3 x mean depth or above 2 x mean depth in each sample and filtered the heterozygous positions with an allele balance below 0.25 or above 0.75 on the basis of hard filtering ("QD<2 | FS>60 | MQ<40 | SOR>3 | ReadPosRankSum<-8.0 MQRankSum < -12.5" for SNPs, and "QD<2 | FS>200 | MQ<40 | SOR>3 | ReadPosRankSum<-20.0" for Indels). The final genome-wide heterozygosity is equal to the number of heterozygous sites divided by the total length of callable regions.

ROHs were calculated based on window-based heterozygosity. First, we generated window-based heterozygosity with a sliding window size of 1Mb size and overlapping size of 200kb. Next, we filtered out the windows with callable region length below 0.5Mb and calculated local minima in the density distribution of window-based heterozygosity. The windows below the median of minima in the same species were identified as autozygous. Finally, we merged the overlapping windows to generate the ROH regions.

Ecological niche modeling

Distribution data for ecological niche modeling

We obtained modern distribution data for 14 gibbon species from the Global Biodiversity Information Facility (GBIF), treating *Nomascus annamensis* and *N. gabriellae* as a single group, and similarly combining *N. siki* and *N. leucogenys*. After removing duplicates and geo-referencing errors using the R package CoordinateCleaner.[124] we retained 1,187 occurrence records across all species, with sample sizes ranging from 10 for Hylobates klossii to 372 for H. lar. To pool occurrence records by gibbon genus and match the resolution of the Krapp et al. paleoclimate dataset,[146] we pooled occurrence records by genus and applied a $0.5^\circ \times 0.5^\circ$ grid filter, randomly retaining a single point per grid cell.

Environmental variables

We downloaded the Krapp et al.[146] paleoclimate dataset (spanning 800 ka BP to the present at 1,000-year intervals) from the pastclim R package (v1.0.4.2),[125] which provides 17 annual climatic variables for each time point. We cropped the dataset to the region between 89° and 120°E and −11° and 30°N to encompass the entire current distribution of gibbons in Southeast Asia. To reduce

multicollinearity and enhance model robustness, we selected a subset of climatic variables with pairwise correlation coefficients below 0.8.

Niche models

To correct sampling bias when generating background points, we used kernel density estimation (KDE) with the rasterize and kde2d functions in raster package to create a bias layer reflecting occurrence density. Background points were then sampled accordingly and combined with occurrence data to build models using the ENMeval package[126] with the maxnet algorithm. Model tuning involved testing multiple feature classes (fc = "L", "LQ", "LQH", "H") and regularization multipliers (rm = 1–5) via cross-validation. The best model was selected based on ΔAICc, average test AUC, and omission rates.[147]

The optimal model was projected onto paleoclimate layers across different time slices to generate continuous suitability maps. To minimize extrapolation artifacts, we computed Multivariate Environmental Similarity Surface (MESS) values and assigned zero suitability to all grid cells with negative MESS values, thereby enforcing conservative predictions. We determined an optimal threshold for converting continuous predictions to binary presence-absence maps by maximizing the balance between true positive rate (TPR) and true negative rate (TNR) from the ROC curve.[148] Using this threshold, we derived binary maps for each time point and calculated average suitability and suitable habitat area per period. We focused on three key time intervals: The Last Glacial Maximum (19-26 kya); Late Middle Pleistocene (65–75 kya), coinciding with population expansions in all four genera; Genus-specific pre-expansion lows (*Hoolock*: 179–189 kya; *Hylobates*: 104–114 kya; *Nomascus*: 167–177 kya; *Symphalangus*: 217–227 kya). For each interval, we averaged continuous suitability predictions to create mean suitability maps, and extracted total suitable habitat area and mean climatic suitability to assess habitat shifts over time.

Structural variant (SV) calling, genotyping and annotation

Gibbon-specific structural variant calling, genotyping, filtering and annotation

We used an assembly-based structural variant (SV) calling pipeline to identify gibbon-specific insertions and deletions. We first aligned the four gibbon genomes to the human reference genome (GRCh38) using minimap2.[96] Next, we used SVIM-asm[97] to call structural variants. After removing imprecise and low-quality SVs, we performed SV genotyping using an alignment-based pipeline. We mapped the raw long reads of the four gibbons (Nanopore or PacBio long reads from our previous published genome assembly data[24]) to the human reference genome (GRCh38) using minimap2 and genotyped the SVs using Sniffles2.[98] To filter out great ape and human-specific SVs and determine the ancestral state of SVs in the superfamily of *Hominoidea*, given our use of the human genome as a reference, we incorporated great ape and macaque genomes. They were individually aligned to the human genome, and we retained only those structural variants where the macaque and great ape genotypes were homozygous for the REF allele. Only SVs that were homozygous for ALT alleles across all four gibbon species and homozygous for REF alleles in great apes and macaques were recognized as gibbon-specific SVs (Table S8). Finally, we used the Ensembl Variant Effect Predictor (VEP)[100] to annotate the consequences of SVs.

Identification of Gibbon-Specific SVs associated with Limb Development

To identify candidates potentially related to limb elongation, we curated a list of 240 genes from the Mouse Genome Informatics (MGI) database (v6.24, retrieved May 2025) associated with Mammalian Phenotype Ontology terms: 'short limbs' (MP:0000547), 'long limbs' (MP:0000548), 'absent limbs' (MP:0000549), 'increased length of long bones' (MP:0004686), and 'decreased length of long bones' (MP:0004686) (Table S9). Gibbon-specific SVs located within or near (e.g., +/- 5kb) these genes were identified using bedtools v2.31.1[94] intersect.

Experiments to study the functional consequences of the structural variant in the SHH gene

Dual-Luciferase Reporter Assay

Dual-Luciferase Reporter Assay was performed using the following vectors: pGL3-promoter-Human-SHH-3'UTR, pGL3-promoter-Human-SHH-3'UTR-Random deletion-1, pGL3-promoter-Human-SHH-3'UTR-Random deletion-2, all synthesized by Beijing Tsingke Biotech Corporation, and the pRL-TK vector obtained from the Key Laboratory of Genetic Evolution & Animal Models. The assay was carried out in SV (from the cell bank of the Kunming Institute of Zoology, Chinese Academy of Sciences) and hBMSCs cells (purchased from Oricell, catalog number HUXMF-01001). 293T cells were cultured in DMEM medium with 10% FBS and 1% penicillin-streptomycin, while hBMSCs cells were cultured in Mesenchymal Stem Cell Complete Medium (Cat. No. HUXMF-90011, Oricell). The cells were maintained at 37°C in a humidified incubator with 5% CO_2. The cells were seeded in 6-well plates (Cat. No. 3516, Corning) at a density of 1×10^5 cells per well. After 24 hours of incubation, the cells were transfected with vectors using Lipofectamine 3000 (Cat. No. L3000015, Invitrogen) following the manufacturer's instructions. In each well, approximately 1250 ng of the recombinant pGL3-promoter vector (target vector) was co-transfected with 1250 ng of the pRL-TK vector. After 48 hours post-transfection, the cells were harvested by adding 500 μL of Cell Lysis Buffer. The firefly luciferase activity in the cell lysates was measured using the Dual-Luciferase Reporter Assay System (Cat. No. 11402ES60, Yeasen) on the Glomax Navigator (Promega) and normalized to Renilla luciferase activity. Each group consisted of 6 replicates, and each experiment was repeated at least three times.

RNA isolation and qRT-PCR

We conducted qRT-PCR analyses on previously constructed stably transfected hBMSCs. Total RNA from hBMSCs was extracted using TRIzol reagent (Thermo scientific, American) and RNeasy mini kit (Qiagen, German) following manufacturer's instructions. In

addition, reverse transcriptase reactions were performed using PrimerScript RT Reagent kit (Vazyme Biotech, China) following manufacturer's instructions. The purity of RNA was determined according to the value OD260/OD280 radio, and all samples had OD values approaching 2.0. Quantitative RT-PCR was performed using the Quantstudio 5 real-time PCR system (Thermo Scientific, USA). The relative amount of each mRNA was normalized to its corresponding GAPDH mRNA, and the mRNA expression levels were calculated by the $2^{-\Delta\Delta Ct}$ method. All primers were designed using the NCBI Pick Primers tool and validated with a solubility curve. The primer sequences are as follows: GAPDH-F: GACAGTCAGCCGCATCTTCT, GAPDH-R: GCCCAATACGACCAAATCCGT; SHH-F: TCTCCA GAAACTCCGAGCGA, SHH-R: CTCCCCGGGGTTTTTGCTT; GLI1-F: CGCCCAGACAGAGTGTCC, GLI1-R: GTCCTTCTGTCCCCA CACTG.

Bulk RNA-sequencing

We performed bulk RNA sequencing on previously constructed stably transfected hBMSCs. Total RNA from hBMSCs was extracted using TRIzol reagent (Thermo scientific, USA) following manufacturer's instructions. RNA-seq library construction and RNA high-throughput sequencing were performed on a PE-150 (Illumina, USA) high-throughput sequencer by Beijing Novozymes Co. For the data analysis part, in brief, Hisat2(v2.2.1)[101] was used first for read mapping, followed by featurecounts (v2.0.1)[102] for quantification, and then the Deseq2 R package (v1.42.1)[127] for differential gene analysis, and the clusterProfiler R package (v4.10.1)[128] for GO enrichment.

ARS staining

Different groups of hBMSCs were seeded in 6-well plates at a density of 5×10^4 per well and replaced with osteoblast differentiation medium. After 7 or 14 days, cells were washed twice with PBS and stained with ARS staining kit for osteogenesis (Beyotime, China) following manufacturer's instructions. At the end of staining, Alizarin red S was dissolved using a 10% solution of cetylpyridinium chloride (ACMEC biochemical, China) at room temperature for 1h. Alizarin red S solution was quantified using a microplate reader at a wavelength of 562 nm.

Micro-CT scanning

Micro-CT scanning was performed in two separate sessions due to instrumental limitations. For in-vivo scanning, we used a high-resolution micro-CT instrument (Hiscan XM, China). We randomly selected 12 transgenic male mice (at age of 6-12 months) and 12 wild-type male mice (at age of 6-12 months) for scanning. Mice were anesthetized with RWD R500 (China) using a 2% isoflurane concentration and immobilized with a specialized holder. Scanning parameters were set at a source voltage of 80 kV, a source current of 100 μA, and a voxel size of 50 μm. The lengths of the humerus, ulna, femur, and tibia were measured using the manufacturer's software SeProcessPro Analyser (v1.0). For in-vitro scanning, another high-resolution micro-CT instrument (NEMO, PINGSENG Healthcare Inc, China) was used to scan the bodies of the same 24 adult mice under the following conditions: a source voltage of 70 kV, a source current of 100 μA, and a voxel size of 110 μm. Post-scanning, data were exported in DICOM format, and 3D models were reconstructed using Stratoven Checkpoint software (Version: 2024.11.14.10:09 WIN x64). The spine length was determined by marking multiple points on the vertebrae and measuring the distance between consecutive points in the 3D models.

Statistical Analysis of Limb Bone Lengths

The average length for each bone type (humerus, ulna, femur, and tibia) was calculated and used as the response variable in all subsequent analyses to account for the non-independence of bilateral measurements from the same individual. Initial comparisons of overall body size (body weight and spine length) between knock-in (KI) and wild-type (WT) groups were conducted using independent two-sample Student's t-tests. To test for differences in relative limb bone length while accounting for significant differences in body size between genotypes, we employed a normalization by covariate approach (the "ratio method"). The average length of each of the four bone types was normalized by dividing it by either the individual's body weight or its spine length. This resulted in two sets of size-corrected ratios for each bone: (1) bone length relative to body weight, and (2) bone length relative to spine length. These ratios were then compared between KI and WT groups using independent two-sample Student's t-tests. A P-value less than 0.05 was considered statistically significant. Effect sizes were quantified to assess the magnitude of the difference in relative limb lengths. The percentage change for each bone was calculated as [(Mean Ratio_KI - Mean Ratio_WT) / Mean Ratio_WT] * 100%. Additionally, the standardized mean difference (Cohen's d) was calculated for each comparison using the effsize package in R to provide a scale-independent measure of effect size. All statistical analyses were performed in R v4.4.0.

Comparative Analysis of SHH Locus Variation in Human Populations

To investigate whether variation at the human SHH locus is associated with limb or body proportion phenotypes, providing a comparative context for our findings in gibbons, we conducted a systematic search of publicly available human genetic and genomic data. First, to identify known associations between genetic variants and relevant traits, we consulted recent large-scale human GWAS literature[70,71] and comprehensively queried the NHGRI-EBI GWAS Catalog[72] and the Open Targets Platform (retrieved June 2025).[73] Our search focused on associations between variants at the SHH locus and the traits 'Height', 'Sitting height', 'Arm length', and 'Leg length'. Second, to search for structural variants (SVs) analogous to the gibbon-specific deletion, we queried major genomic variant databases, including the Database of Genomic Variants (DGV) (v107)[74] and gnomAD-SV (v4.1.0),[75] for indels or CNVs within the human SHH 3'UTR.

Supplemental figures

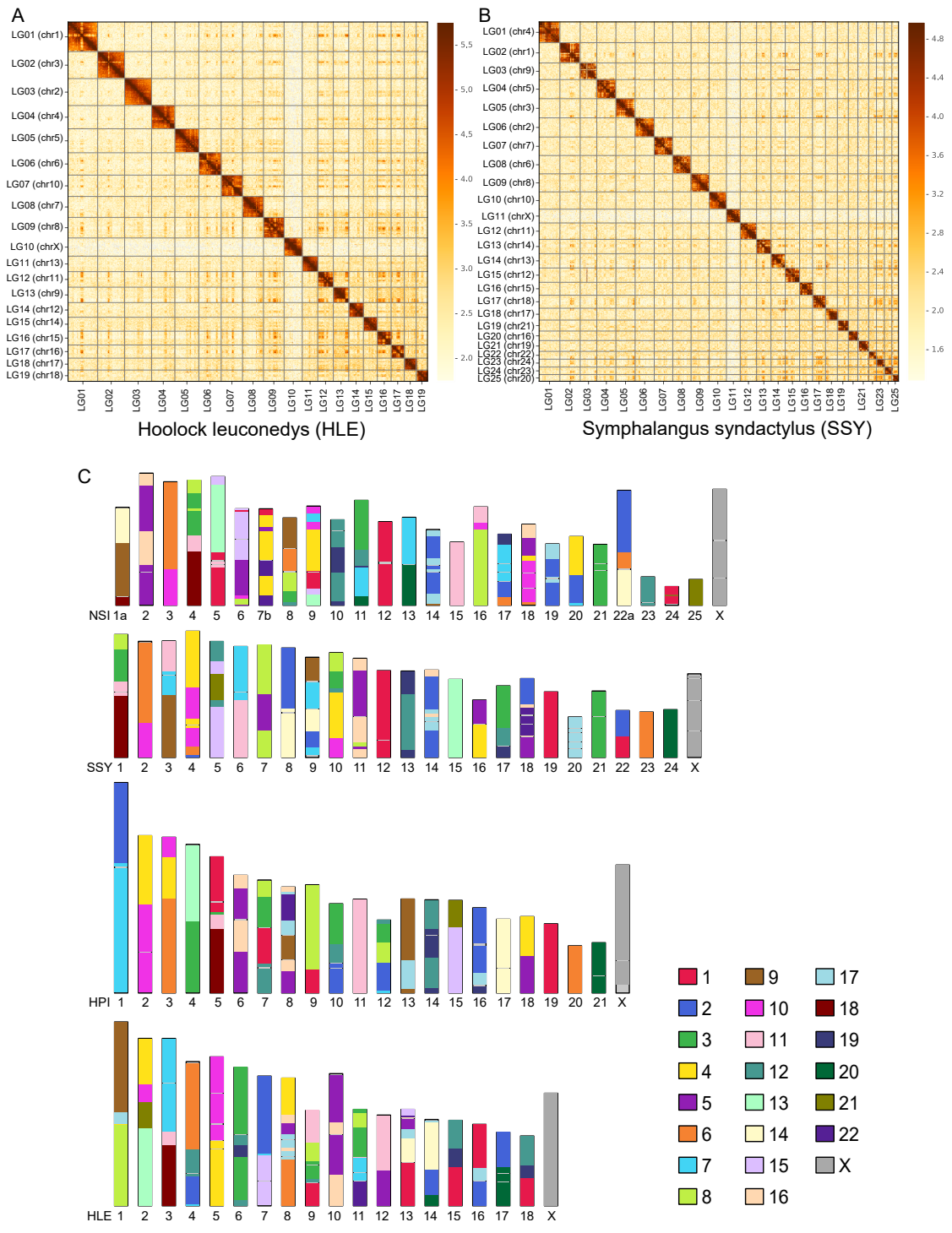

(legend on next page)

Figure S1. Gibbon genome scaffolding with Hi-C and synteny with human, related to Figure 1 and Table 1

(A) Heatmap plot of genome-wide all-vs.-all Hi-C interaction of *Hoolock leuconedys* (HLE) at a resolution of 500 kb.

(B) Heatmap plot of genome-wide all-vs.-all Hi-C interaction of *Symphalangus syndactylus* (SSY) at a resolution of 500 kb.

(C) Synthesis between the chromosomes of four gibbon genomes and human. Colors in the gibbon chromosomes present homologs to parts of the human chromosomes of the same color in the bottom right legend.

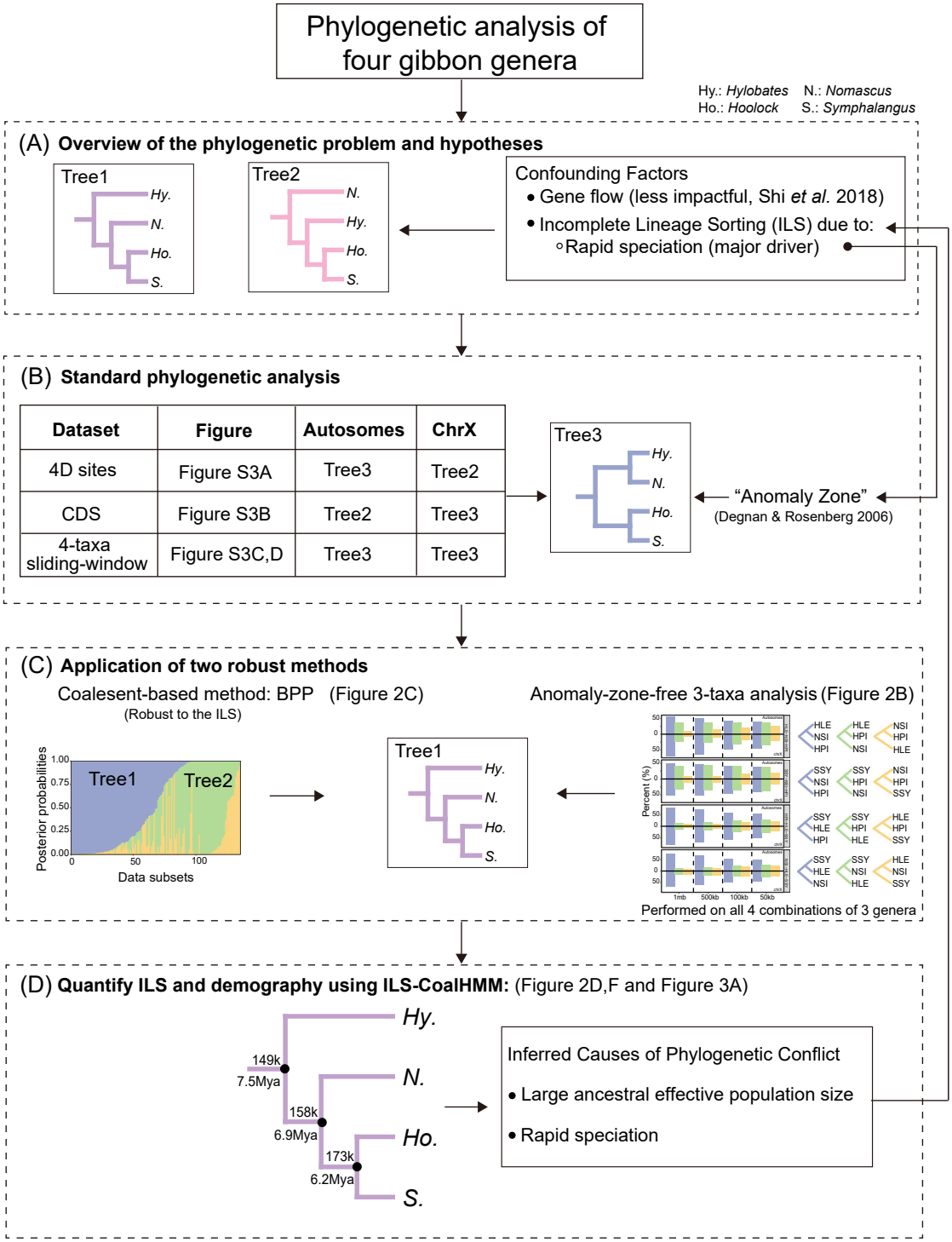

Figure S2. Flowchart of the integrated phylogenetic analysis to resolve the gibbon genus-level species tree, related to Figure 3

(A) Overview of the phylogenetic problem and hypotheses. The phylogeny of the four gibbon genera has been contentious, with two main competing hypotheses, Tree1 and Tree2. The primary confounding factor is extensive incomplete lineage sorting (ILS) caused by a rapid speciation event, which complicates phylogenetic inference.

(B) Standard phylogenetic analysis. This shows that concatenation-based methods are highly inconsistent, yielding different majority-supported topologies (Tree2 and Tree3) depending on the dataset. The high frequency of balanced trees in sliding-window analyses indicated that the phylogeny resides within the "anomaly zone," a theoretical condition where standard methods are known to be unreliable.

(legend continued on next page)

(C) Application of two robust methods. To overcome the challenges of the anomaly zone and ILS, we employed two independent and theoretically robust methods as our primary criteria for species tree inference. Coalescent-based method (BPP): this method explicitly models ILS to directly estimate the posterior probability of the species tree. Anomaly-zone-free 3-taxa analysis: this approach leverages the theoretical principle that three-taxon phylogenies are immune to the anomaly zone. By analyzing all possible three-taxon subsets, we could infer the overarching four-taxon relationship without being misled by anomalous gene trees. Both robust methods converged on the same conclusion. The BPP analysis (Figure 2C) provided a powerful quantitative measure of uncertainty, resolving Tree1 as the species tree with a posterior probability of ~0.48. Independently, the 3-taxa analysis (Figure 2B) showed that only topologies consistent with Tree1 were the most frequent across all combinations.

(D) Quantify ILS and demography using ILS-CoalHMM. Based on this convergent and statistically robust evidence, Tree1 was confidently adopted as the species tree. It was subsequently used in the ILS-CoalHMM analysis to quantify the extent of ILS and infer demographic parameters, confirming that large ancestral effective population sizes and rapid speciation lead to the high level of ILS.

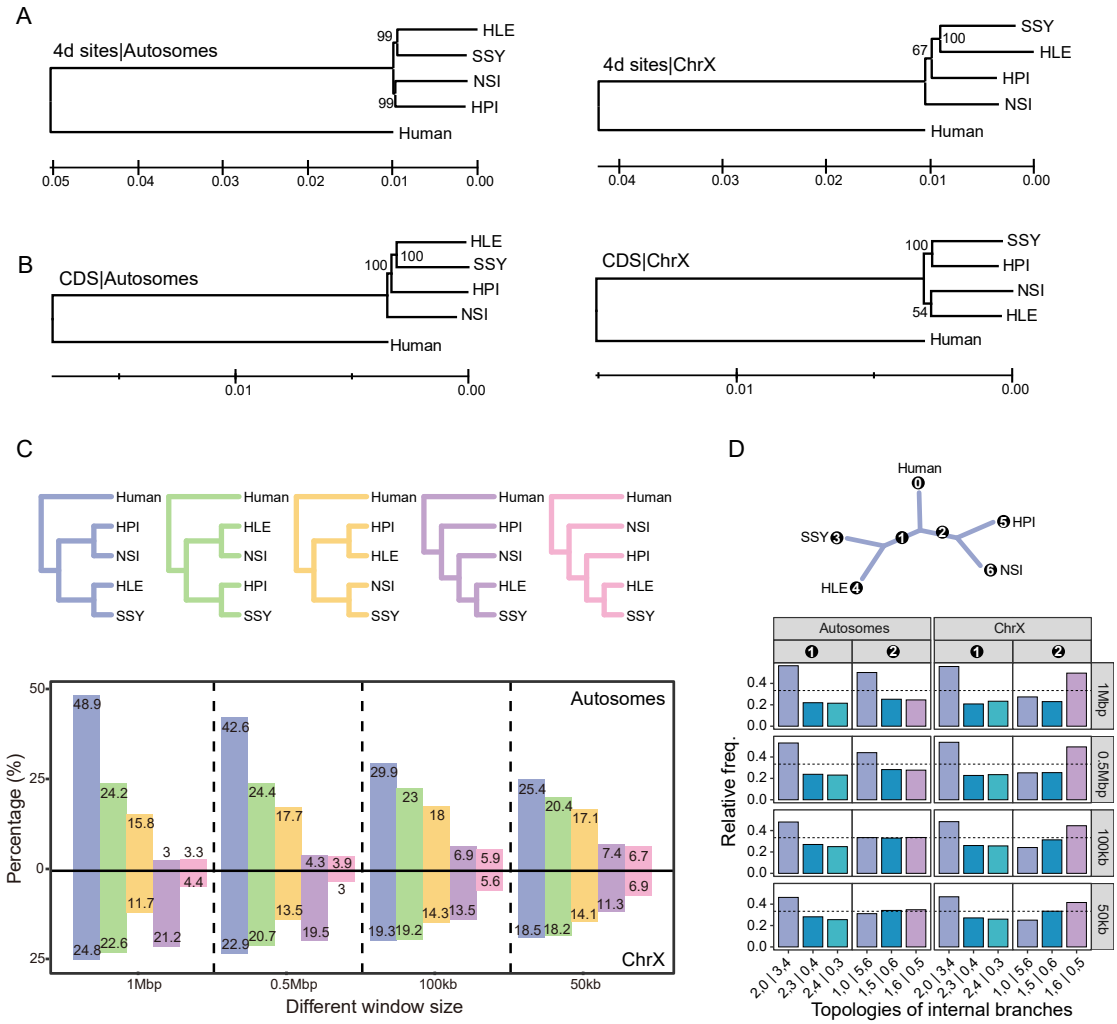

Figure S3. Phylogeny between the four gibbon genera, related to Figure 2

(A) Maximum-likelihood (ML) phylogenetic tree based on 4d sites (~4.9 Mb for autosomes and ~0.18 Mb for the X chromosome).

(B) ML phylogenetic tree from CDS (~10.0 Mb for autosomes and ~0.34 Mb for the X chromosome).

(C) Percentage of the top five tree topologies based on four different window sizes and five-taxa groups across all autosomes and the X chromosome. Colors in the bar plots and phylogenetic trees refer to the same tree topology.

(D) DiscoVista plot based on four different window sizes and five-taxa groups across all autosomes and the X chromosome.

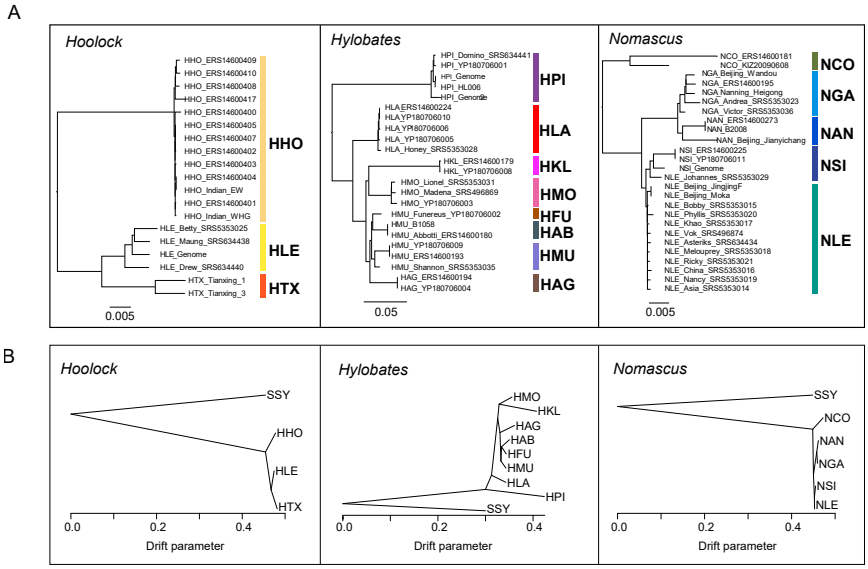

Figure S4. Phylogeny within three gibbon genera, related to Figure 3

(A) Neighbor-joining trees across three genera using whole-genome SNP datasets (removing the outgroup of siamang for plotting).

(B) Maximum-likelihood (ML) trees across three genera using whole-genome SNP datasets. The support rate of each node is 100% using 100 bootstrap replicates.

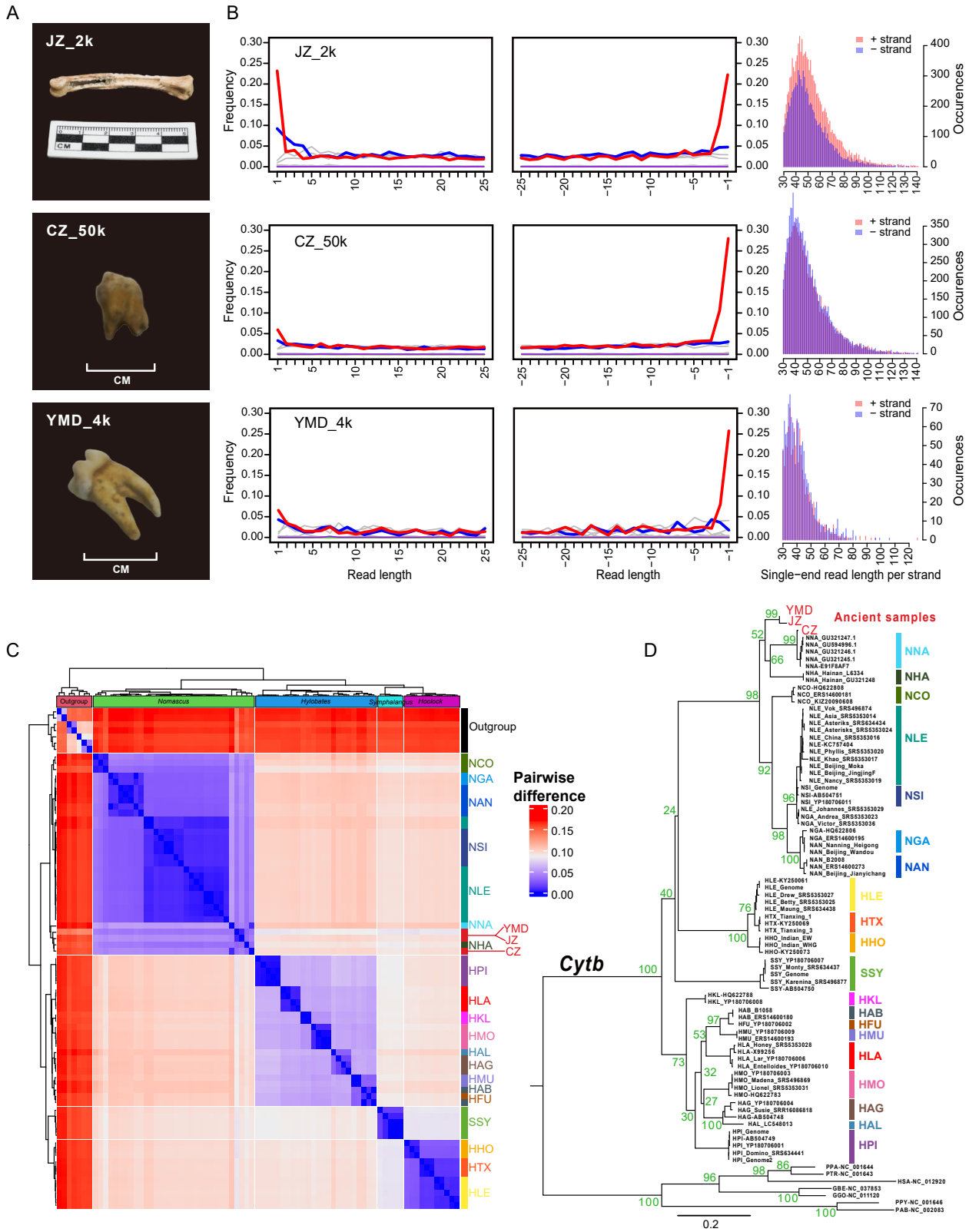

(legend on next page)

Figure S5. Three ancient gibbon samples and their relationship with extant gibbons, related to Figure 4

(A) Photos of the sample material from the three ancient gibbon specimens. YMD_4k is from Yemao Cave, Qijiang District, Chongqing, China. CZ_50k is from Longlinshan Cave, Manluxincun, Chongzuo, Guangxi Province, China. JZ_2k is from the Shenheyuan tomb (from a ~2,200- to 2,300-year-old tomb possibly belonging to Lady Xia, grandmother of China's first emperor, Qin Shihuang (259–210 BCE), Changan District, Shaanxi Province.

(B) Plots of deamination patterns and the histograms of the read lengths made with MapDamage. The plots in the left two columns are positions at the specific substitutions from the 5′ (left) and the 3′ ends (right), and from top to bottom are the deamination patterns of JZ_2k (*Junzi imperialis*), CZ_50k, and YMD_4k gibbon. Here, the red color is the C-to-T substitutions, and blue is the G-to-A substitutions, which together show the characteristics of the ancient DNA sequencing. Gray color means other substitutions. The right shows the single-end read length per strand.

(C) Heatmap and hierarchical clustering dendrogram based on the pair genetic divergence of complete mitochondrial genomes.

(D) ML tree based on the mitochondrial *Cytb* gene sequences.

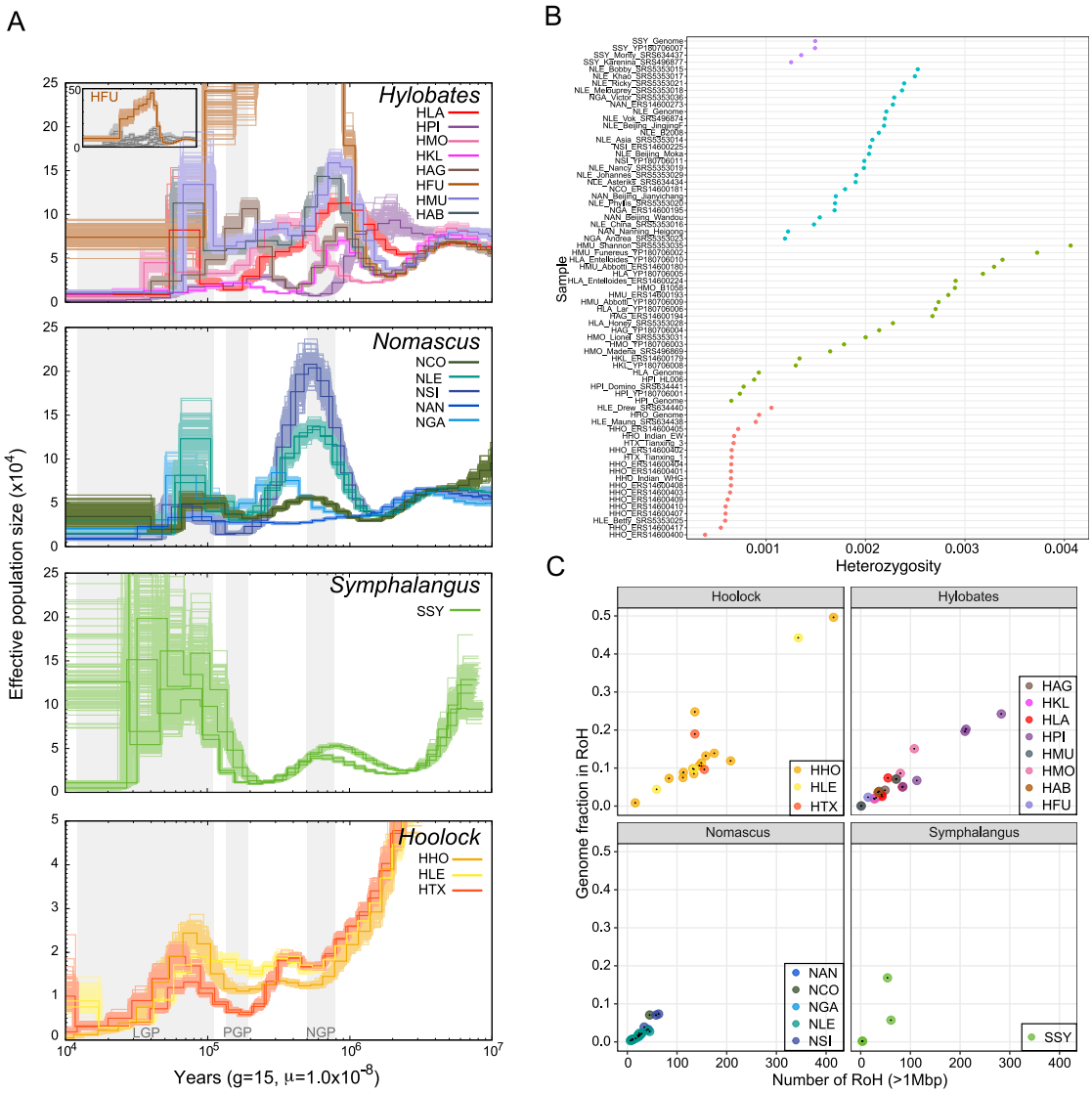

Figure S6. Historical population dynamics and contemporary genetic diversity of gibbons, related to Figure 5

(A) Historical effective population size (N_e) trajectories of individual gibbon species inferred by PSMC. Each line represents the demographic history of a single individual, with plots grouped by genus. The *y* axis shows N_e (scaled by 10^4), and the *x* axis shows time in years before present on a log scale (assuming g = 15 years, mu = 1.0×10^{-8}). The thin, lighter lines represent 100 bootstrap replicates for each analysis. Gray shaded vertical bars indicate the approximate timings of major glacial periods: the Last Glacial Period (LGP, ~12–110 kya), the Penultimate Glacial Period (PGP, ~135–194 kya), and the Naynayxungla Glacial Period (NGP, ~500–780 kya). The inset in the Hylobates panel provides a magnified view of the HFU trajectory.

(B) Genome-wide heterozygosity for all sequenced gibbon individuals. Each point represents the heterozygosity of one individual, grouped and colored by genus. The *x* axis shows the fraction of heterozygous sites per base pair.

(C) Runs of homozygosity (RoHs) analysis across gibbon species. Each point represents one individual, plotted by the total number of RoH segments ≥1 Mbp (*x* axis) and the fraction of the genome contained within these RoH segments (*y* axis). Plots are faceted by genus, with different species indicated by color as per the legend.

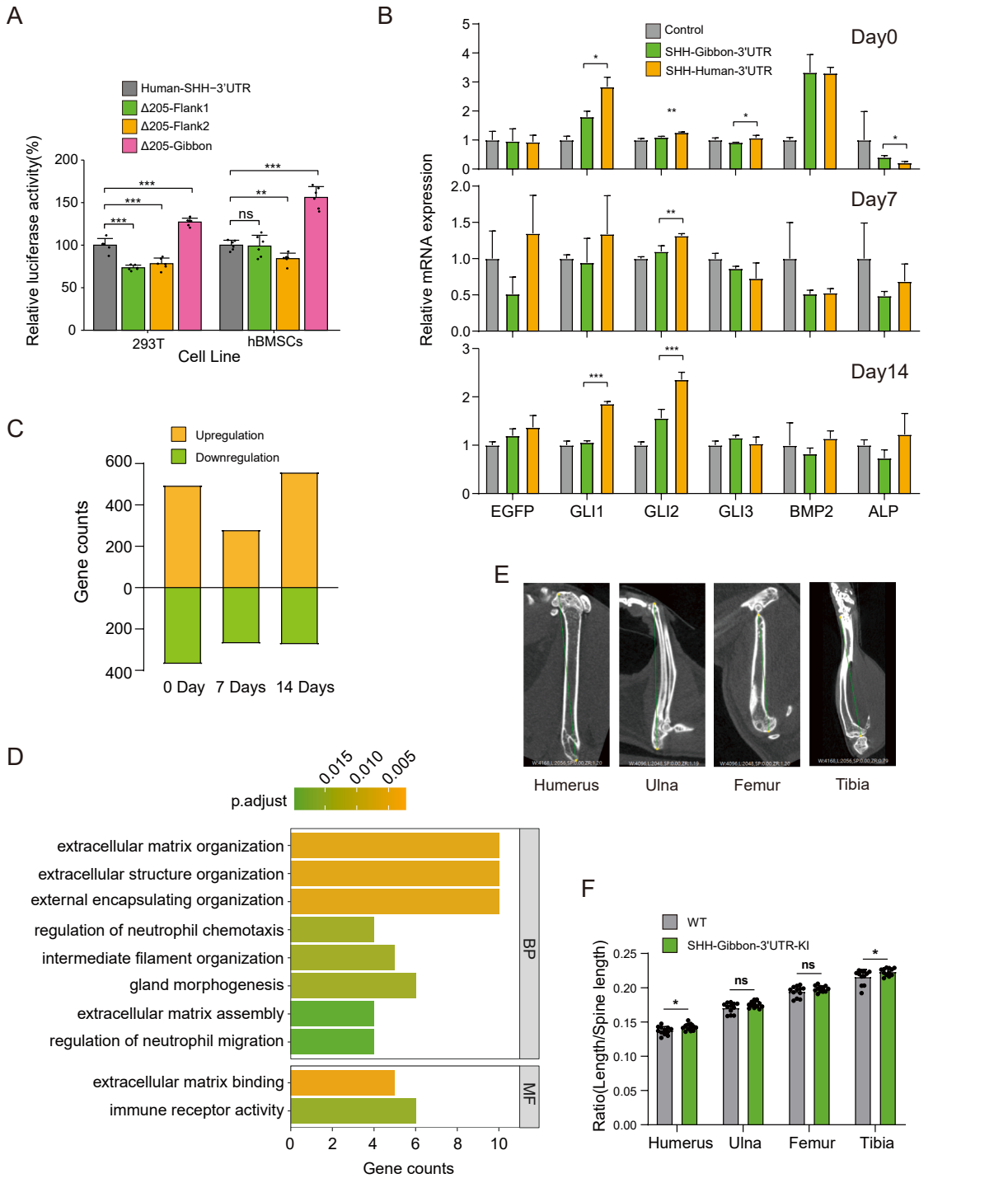

Figure S7. The cellular and *in vivo* functional analyses of the SHH 3′ UTR deletion, related to Figure 6

(A) Luciferase reporter assays in 293T and hBMSC lines showing the specific regulatory effect of the Δ205-Gibbon deletion compared with WT and two identically sized flanking region deletion controls (Δ205-Flank1 and Δ205-Flank2).

(B) Relative mRNA expression of key genes during osteogenic differentiation of hBMSCs. Expression levels of the EGFP reporter and downstream Hedgehog pathway components (GLI1, GLI2, and GLI3) and osteogenic markers (bone morphogenetic protein 2 [BMP2] and alkaline phosphatase [ALP]) were measured by RNA sequencing at days 0, 7, and 14.

(C) Number of differentially expressed genes (DEGs) between hBMSCs expressing the gibbon vs. human SHH 3′ UTR at different time points during differentiation. Bars show the counts of significantly upregulated (orange) and downregulated (green) genes in the gibbon-3′ UTR cell population.

(legend continued on next page)

(D) Gene Ontology (GO) enrichment analysis of the DEGs. The bar plot shows the top enriched GO terms in the biological process (BP) and molecular function (MF) categories, with bar color indicating the adjusted *p* value.
(E) Representative micro-CT images of the four major limb bones (humerus, ulna, femur, and tibia) from a KI mouse, illustrating the method for bone length measurement.
(F) Relative limb bone lengths normalized by spine length. Bar charts show the ratio of each bone's length to the individual's spine length for wild-type (WT) and KI mice.
Statistical significance was determined by Student's *t* test (for A, B, and F). ns, not significant; $^{*}p < 0.05$, $^{**}p < 0.01$, $^{***}p < 0.001$.